Extreme Light Physics and Application

Nobel Lecture, December 8, 2018 by
Gérard Mourou
University of Michigan, Ann Arbor, MI, USA & École Polytechnique, Palaiseau, France.

I. INTRODUCTION

The advent of ultraintense laser pulses generated by the technique of chirped pulse amplification (CPA), along with the development of high-fluence laser materials has opened up entirely new fields of optics. A CPA laser exhibits stunning capabilities. It can generate the largest field, the largest pressure, the highest temperature and accelerating field, making it a universal source of high energy particles and radiation.

CPA technology produces a wide range of intensities extending from 10^{14} to 10^{25} W/cm^2. In the lower part of this range, the intensity regimes of 10^{14} to 10^{17} have applications that include micromachining, which can be performed on material regardless of its nature, i.e. ceramic, metal, biological tissue, cornea, etc. Extremely clean cuts of minimal roughness even at the atomic scale are produced. This attractive property led us to applications in ophthalmic procedures like refractive surgery, cataract surgery, corneal transplants and glaucoma treatment. Today, a million patients a year are benefiting from femtosecond interventions. In science, in the same intensity level, CPA makes possible to reach the attosecond frontier, offering a formidable tool to time resolved fundamental electronic processes.

For intensities >10^{18} W/cm^2 laser-matter interaction becomes strongly dominated by the relativistic character of the electron. In contrast to the nonrelativistic regime, the laser field moves matter more effectively, including motion in the direction of laser propagation, nonlinear modulation and harmonic generation, leading to high energy particle and radiation production. One of the hallmarks of this regime is Laser Wakefield Acceleration (LWA), where the electromagnetic energy from a laser pulse is transformed into kinetic energy producing accelerating gradients a thousand times higher than those applied in conventional accelerators. The electron beam can, in turn, produce a copious amount of keV radiation by betatron or Compton scattering.

For intensities at 10^{25} W/cm^2 the laser field becomes so large that protons and ions become relativist with GeV energies. The acceleration is directly produced by the light pressure. The source size is very small, and the large acceleration gradients combine to make this source brightness better than any existing.

The coupling of an intense laser field to matter also has implications for the study of the highest energies in astrophysics, such as ultrahigh-energy cosmic rays with energies in excess of 10^{20} eV. Intense laser fields can also produce an accelerating field sufficient to simulate general relativistic effects in the laboratory via the equivalence principle like the loss of information in Black Holes.

Many CPA applications offer great benefit to humankind. We discuss a few examples capitalising on the compactness of the CPA-based source. For instance, the generation of high energy protons and neutrons applied to the treatment of cancer, i.e proton therapy, or in nuclear pharmacology where short-lived radionuclides could now be created for therapy or diagnostics near the patient's bed.

In the environmental arena, owing to the efficient generation of high energy neutrons, it is one of our goals to use them to shorten the degree of radiotoxicity of the most dangerous elements, the minor actinides in nuclear waste.

Finally, looking onwards, particle production in "empty" space will remain one of the main objectives of the field. It is the historical path which guided the field in order to acquire an understanding of fundamental questions on the structure of vacuums, to give us a glimpse of the propagation of light in vacuums and how it defines the mass of all elementary particles.

A novel laser architecture to reach intensities at the Schwinger level is explored. Its paradigm is based on the transition of a single cycle visible light pulse into a high energy single cycle X-ray pulse. Successful transposition would give the field a formidable boost, equivalent to the one received when maser transitioned into laser, moving from GHz to PHz (Light) frequencies.

II. THE CPA TECHNIQUE

The key to high and ultrahigh peak power and intensity is the amplification of ultrashort pulses in the picosecond and femtosecond time scales. Over the past 40 years laser-pulse durations have continuously decreased from the microsecond domain with free running to the nanosecond regime with Q-switching, and finally to the picosecond and few-femtosecond regime with mode locking (Brabec and Krausz, 2000). With the advent of mode locking, the laser-pulse duration became so short that pulses could not be amplified without producing unwanted nonlinear effects. This caused a power and intensity plateau seen in Fig. 1. Before 1985, for reasonable sized systems, i.e., with a beam diameter of the order of 1 cm, the maximum obtainable power remained around 1GW, with focused intensities of about 10^{14} W/cm^2. Higher power could be obtained through the use of amplifying media with gain bandwidths that can accommodate the short pulse spectrum and high-energy storage media that have a small transition cross section σ_a. However, to be efficient, this approach requires the use of input pulses with a high laser fluence of a few J/cm^2. As we shall see later, good energy extraction from an amplifier calls for input pulses close to the saturation fluence, see Eq. 1. This level of fluence delivered over a short time leads to prohibitively large intensities, in excess of TW/cm^2. This is far above the limit of the GW/cm^2 imposed by the need to prevent nonlinear effects and optical damage in the amplifiers and optical components. As a result, the only alternative seemed to use low-energy storage materials such as dyes or excimers and increase the laser beam cross section. The latter is unattractive as it leads to large, low-repetition rate and costly laser systems. Therefore, high-intensity physics research was limited to a few large facilities such as the CO2 laser at Los Alamos National Laboratory (Carman et al., 1981), the Nd:glass laser at the Laboratory for Laser Energetics (Bunkenburg et al., 1981), and excimer lasers at the University of Illinois at Chicago and University of Tokyo (Luk et al., 1989; Endoh et al., 1989).

In 1985 laser physicists at the University of Rochester (Strickland and Mourou, 1985) and later (Maine and Mourou, 1988; Maine et al., 1988), demonstrated a way to simultaneously accommodate the very large beam fluence necessary for energy extraction in superior storage materials while keeping the intensity and nonlinear effects to an acceptable level. This technique was called Chirped Pulsed Amplification (CPA). CPA revolutionised the field in three ways. First, a TW system could fit on a tabletop, thus delivering intensities 10^5–10^6 times higher utilising conventional technology. Second, the CPA architecture could be easily retrofitted to existing large laser fusion systems at relatively low cost. Today CPA is incorporated in all the major laser fusion systems around the world such as: Japan (Yamakawa et al., 1991), France (Rouyer et al., 1993), United

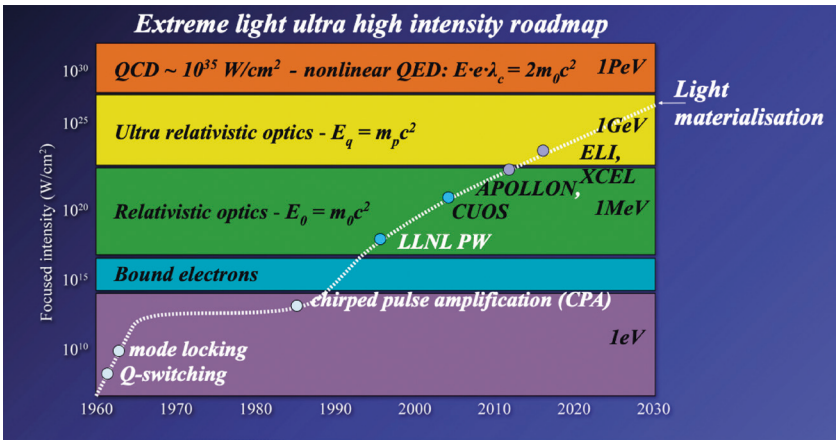

Figure 1. Laser intensity vs years.

Kingdom Vulcan Laser, United States Perry et al., 1999, etc. Third, because of their reduced size CPA lasers could be combined with large particle accelerators. In the case of synchrotrons (Wulff et al., 1997; Larsson et al., 1998; Schoenlein et al., 2000), they could be used to study time-resolved x-ray diffraction. With a linear collider such as SLAC one could produce fields higher than the critical field (Bula et al., 1996) and observe nonlinear QED effects such as pair generation from a vacuum. At present all the colliders are considering the incorporation of CPA technology to produce γ rays for photon-photon collisions to produce a γ-γ collider, (Telnov, 1990, 2000, 2001; Yokoya, 2000).

As we shall describe later, the availability of ultra-high intensity lasers has extended the horizon of laser physics from atomic and condensed-matter studies to plasma, nuclear, and high-energy physics, general relativity, cosmology, and physics beyond the standard model. It has also had a major effect in bringing back to university laboratories science that formerly could only be studied with large-scale facilities. Also at a relatively low peak power level, it made precision machining and ophthalmic procedures in the medical arena possible.

A. Amplification: The Energy Extraction Condition

Before 1985 all amplifier systems were based on direct amplification. As mentioned in the introduction, for extraction efficiency, a simple rule is that the energy per unit area be of the order of F_{sat}, the saturation fluence of the materials. This value is given by

$$F_{sat} = \frac{\hbar\omega}{\sigma_a} \qquad (1)$$

where ħ is Planck's constant, ω is the angular laser frequency and σ_a is the amplifying transition cross section. F_{sat} is 0.9 J/cm^2 for Ti:sapphire and 4 J/cm^2 for Nd:glass and of the order of a mJ/cm^2 for dyes and excimers. It can be shown (Siegman, 1986) the output fluence F_{out} is given by

$$F_{out} = F_{sat} \ln\left[\frac{G_0 - 1}{G(t) - 1}\right] \qquad (2)$$

where G_0 is the low signal gain and

$$G(t) = \exp\left[\sigma N_{tot}(t)\right] \qquad (3)$$

$$\eta = \left[\frac{\ln G_0 - \ln G_f}{\ln G_0}\right] \qquad (4)$$

The gain G_f at the end of the impulsion is given by

$$G_f = 1 + (G_0 - 1)\exp\left[-\frac{F_{pulse}}{F_{sat}}\right] \qquad (5)$$

From Eqs. 4 and 5 we see that, to reach an efficiency close to unity, the laser input fluence F_{pulse} must correspond to few times F_{sat}. Fig. 2 illustrates this point for two different initial gains G_0 of 10 and 10^3.

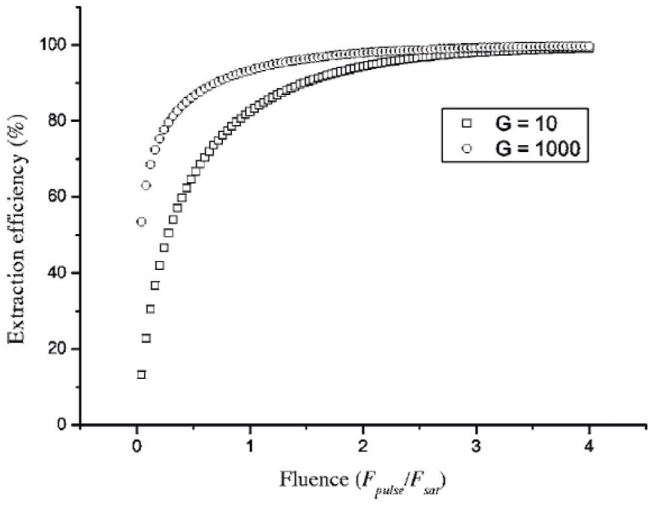

Figure 2. Amplifier efficiency. This illustrates the importance for the input pulse fluence Fpulse to be few times the saturation fluence F_{sat} to obtain a good extraction efficiency.

B. Amplification: The Propagation Condition

Prior to CPA the amplifying media were exclusively dyes, (Migus et al., 1982) and excimers (Endoh et al., 1989; Luk et al., 1989). Typical cross sections for these media are very large, in the range of 10^{-16} cm^2, implying a F_{sat} of only a few mJ/cm^2, or a power density of 1 GW/cm^2 for subpicosecond pulses. At this power density level, the index of refraction becomes intensity dependent according to the well-known expression

$$n = n_0 + n_2 I \qquad (6)$$

Due to the spatial variation of the laser beam intensity, this will modify the beam wavefront according to the B integral given by

$$B = \frac{2\pi}{\lambda} \int_0^L n_2 I(x) dx \qquad (7)$$

Here, B represents, in units of λ, the amount of wavefront distortion due to the intensity-dependent index of refraction, accumulated by the beam over a length L. For a perfectly Gaussian beam, B will cause the whole beam to self-focus above a critical power given by

$$P = \frac{\lambda_0^2}{2\pi n_0 n_2} \qquad (8)$$

For a nonlinear index $n_2=5\times10^{-16}cm^2/W$ for Ti:sapphire. When the laser beam exhibits spatial intensity modulations, n_2 will cause the beam to break up in filaments. In practice the small scale self-focusing represents the most severe problem in an amplifier system. The maximum growth rate g_m (Bespalov and Talanov, 1966) will occur for spatial frequencies K_m given by

$$K_m = \left(\frac{2\pi}{\lambda}\right)\left(\frac{2n_2 I}{n_0}\right)^{1/2} \qquad (9)$$

$$g_m = \left(\frac{2\pi}{\lambda}\right)\left(\frac{n_2 I}{n_0}\right) \qquad (10)$$

For intensities of the order of $I = 1\ GW/cm^2$ in Ti:sapphire, $K_m=200\ cm^{-1}$, corresponding to 50 μm spatial wavelength. As seen in Fig. 3, these wavefront "irregularities" will grow at a rate of $g_m= 3\ cm^{-1}$ with an exponential growth rate G_m over the gain length L exactly equal to B,

$Gm = B$

For laser fusion, the beam is "cleaned" with spatial filters every time B reaches 3. For high-field experiments in which the spatial and temporal beam quality requirements are more stringent, B must be kept below 0.3 corresponding to a wavefront distortion of λ/20.

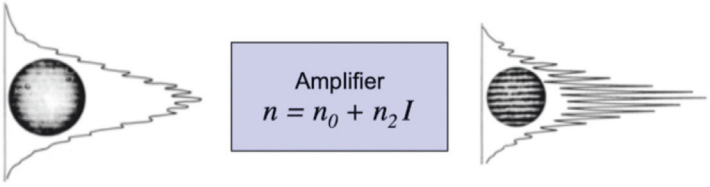

Figure 3. The intensity dependence of the Index of refraction, will create spatial variation of the laser beam intensity, producing undesirable filaments and hot spot.

C. The CPA Concept

We have seen that amplifying media with low cross sections offer the benefit of compactness. For instance, Nd:glass has a cross section of 10^{-21} cm^2, which means that we can store 10^3 to 10^4 times more atoms per unit volume and consequently, get 10^3 to 10^4 more energy before it self-oscillates, than with a dye or excimer with cross section 10^{16} cm^2. However, to extract all the energy in a picosecond pulse would require a beam with a fluence F_s of the order of 1 J/cm^2 or an intensity of 10^{12} W/cm^2 corresponding to a B of 10^3, or 10^3 times the acceptable value.

Therefore, in order to utilise superior energy storage materials, the laser scientist is confronted with the seemingly insoluble dilemma of increasing the input energy needed for energy extraction, while keeping the input intensity at an acceptable level. This problem was solved by the CPA concept. First the pulse is stretched by a factor of 10^3 to 10^4. This step does not change the input pulse energy and therefore does not affect the energy extraction capability, but it does lower the input intensity by the stretching ratio and hence keeps B to a reasonable level. Second, the pulse is amplified by 6 to 12 orders of magnitude, i.e. from the nJ to the millijoule or kilojoule level, before it is finally recompressed by the stretching ratio back to a duration close to its initial value, see Fig. 4.

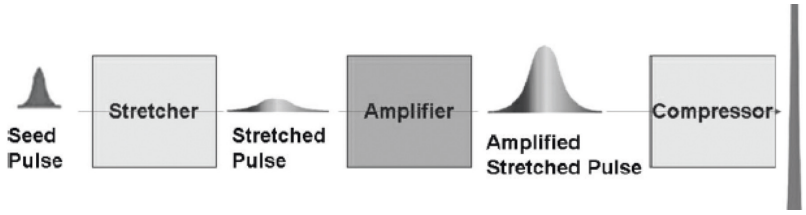

Figure 4. Chirped pulse amplification concept. To minimise nonlinear effects the pulse is first stretched several thousand times lowering the intensity accordingly without changing the input fluence J/cm2. The pulse is next amplified by a factor of 106–1012 and is then recompressed by a factor of several thousand times closer to its initial value.

D. The Key Element: The Matched Stretcher-Compressor

In the first CPA set up (Strickland and Mourou, 1985) the laser pulse was stretched using an optical fibre with a positive group delay dispersion and was recompressed by a pair of parallel gratings (Treacy, 1969), with a negative group delay dispersion. Although this first embodiment led to a spectacular 100-fold improvement in peak power, the problem was that the stretcher and compressor were not matched over all orders. As a result, after recompression the pulse exhibited unacceptable pre-pulses and post-pulses.

This led the Rochester group to look for the ideal "matched stretcher-compressor." It came in 1987, when Martinez (Martinez, 1987) proposed a grating compressor with positive group delay dispersion for communication applications as shown in Fig. 5. In communication systems the wavelength of choice is 1.5 μm, a spectral region where the fibre exhibits negative group velocity dispersion. After propagation in a fibre the bits of information exhibit a negative chirp. It is therefore necessary to use a dispersive delay line after propagation with a positive group velocity dispersion to recompress the pulses. After examining this arrangement, the Rochester group came to the conclusion that the Martinez "compressor" was in fact the matched stretcher of the Treacy compressor that they were intently seeking. This can be easily shown by considering the arrangement shown in Fig. 5. When one uses a telescope of magnification 1, the input grating located at a distance f from the first lens will be imaged at the same distance.

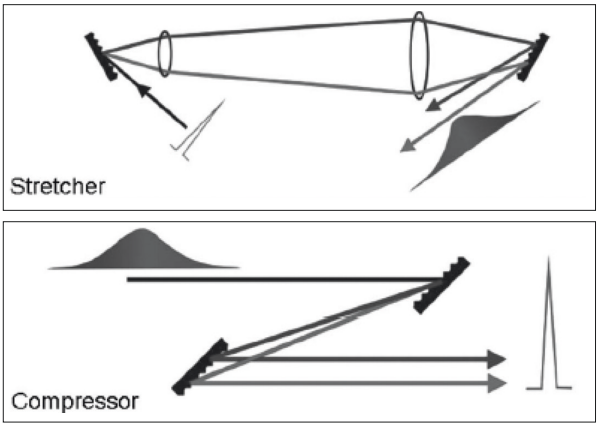

Figure 5. Treacy and Martinez grating arrangements. The Martinez grating pair used as a stretcher and Treacy grating pair used as a compressor. It was discovered and demonstrated by Pessot *et al.*, (1987) that these two grating arrangements are in fact matched over all orders. The pulse can be stretched and recompressed arbitrarily keeping the initial pulse unchanged. This grating arrangement is used in most CPA systems.

The phase conjugation properties of the ''stretcher/compressor'' were proposed and demonstrated in (Pessot et al., 1987) by stretching a pulse of 80 fs by a factor of 1000 using the Martinez arrangement and then compressing it back to exactly the same value using the Treacy compressor.

This demonstration represented a major step in chirped pulse amplification. This matched stretcher-compressor integrated into a CPA system was

to produce the first terawatt pulse on a table top system, the so-called T^3 by the Rochester group. It was subsequently used for subpicosecond pulse amplification (Maine and Mourou, 1988; Maine et al., 1988) and for a pulse duration of 100 fs by Pessot et al. (1989). This arrangement stands today as the standard architecture used in CPA systems.

E. New Materials for CPA, OPCPA and Gain Narrowing

CPA was demonstrated initially with the two broadband-amplifying media that were available at the time, Nd:glass and alexandrite (Pessot et al., 1989). Shortly after, this initial work the concept was extended to Ti:sapphire (Vaillancourt et al., 1990; Kmetec et al., 1991; Squier et al., 1991; Sullivan et al., 1991) as well as Cr:LiSrAlF6 (Beaud et al., 1993; Ditmire and Perry, 1993) and Yb:glass (Nees et al., 1998). Among these materials Ti:sapphire has the advantage of the broadest bandwidth, with a high damage threshold and excellent thermal conductivity greatly enhanced at cryogenic temperatures (Backus et al., 1997).

Parametric amplifiers have also been proposed and demonstrated by Dubietis et al. (1992). It was used for large scale laser applications at the Rutherford Appleton Laboratory (Ross et al., 1997, 2000). This elegant technique, called OPCPA for Optical Parametric Chirped Pulse Amplification, is able, if the nonlinear propagation effects are kept under control, to provide an extremely large gain bandwidth. It offers the great advantage to be pumped by large-scale laser systems dedicated to laser fusion. OPCPA could be the natural companion of any large laser fusion system. A more detailed discussion of the OPCPA method is provided below.

In a conventional CPA system, one of the limitations in pulse duration comes from gain narrowing. Because of their wide spectrum, short pulses can be amplified only by materials with a gain bandwidth greater than the pulse spectrum. We note that materials with superior energy storage typically have a low transition cross section and broad gain bandwidth. However, large gain will lead to a reduction of the laser spectrum as it is amplified and therefore a longer output pulse. In the unsaturated regime – the linear regime – the laser spectrum will be subjected to a narrowing given by

$$G(\omega_a)\,\Delta\omega = \Delta\omega_a \sqrt{\frac{3}{G(\omega_a)-3}} \qquad (11)$$

where $\Delta\omega_a$ is the gain bandwidth and $G(\omega_a)$ the exponential gain. A gain of ten orders of magnitude will narrow the gain bandwidth by a factor of 3 to 4. A fraction of this gain, however, can be recovered in the saturated section of the amplifier.

F. "CAN" a Novel Architecture

Many applications involving high peak power, like high energy particle acceleration or transmutation of nuclear waste crucially need average power. They typically need peak power in the PW range with MW average power and excellent efficiency near 50%. Right now, a typical laser provides PW peak power but only with around tens watts average power and 0.1% efficiency. A far cry from what we would need for real applications.

To mitigate this problem, we proposed to build a novel amplifier based on a multitude (network) of phased fibres, called Coherent Amplifying Network (CAN). In a CAN fibre amplifier (Fig. 6) the active gain medium is confined within the core of the optical fibre. Fibres benefit from efficient heat removal due to the advantageous volume to lateral surface area. It can also be pumped efficiently by a laser diode that is well-tuned to the fibre. Hence the CAN laser could provide simultaneously, peak power, average power and efficiency. Continuous-wave fibre lasers with average powers in the kilowatt regime were first demonstrated in 2004.

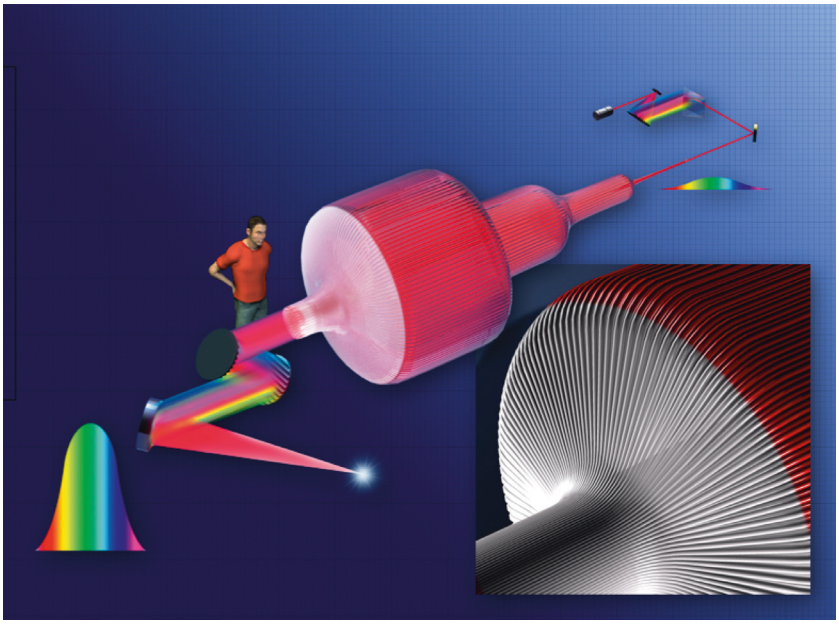

Figure 6. CAN system is a fibre-laser based system built out of thousands of fibre lasers coherently added to increase the average power and pulse energy linearly. The fibre laser offers excellent efficiency (>30%) thanks to laser-diode pumping and provides a much larger surface cooling area, therefore making operation at high peak power and high average power possible with good efficiency and pristine beam quality.

Note also that CAN uses the CPA concept. An initial pulse from an oscillator laser is stretched and split into many fibre channels as many as 104. Each channel is amplified in several stages, with the final stages producing pulses of ~1 mJ at a high repetition rate. All the channels are combined coherently, compressed and focused to produce a pulse with a possible energy of >10 J at a repetition rate of 10 kHz. Of course, the cost of the system will be expensive but at this level any system will have a significant cost.

G. The Quest for PW Peak Power

As soon as the CPA concept was demonstrated at the millijoule and joule levels, it became clear that it could be extended to much higher energies using already built laser fusion systems to amplify nanosecond pulses in the 100–1000 J range. This means that with remarkably few alterations, that is, by chirping the pulse at the input and compressing it at the output, a laser chain built to produce TW with ns duration pulses could now produce petawatt PW with ps duration pulses (Maine et al., 1987).

The first experiment started at the CEA-Limeil on the oldest laser fusion system P102 in the early 1990s. The laser was capable of producing on the order of 100 joules in the nanosecond regime. A seed pulse provided by an oscillator was stretched amplified to several tens of joules and compressed to its initial value with the grating pair compressor. Of course, the main difficulty was the fabrication of the gratings with a decent damage threshold and efficiency that could handle the large pulse energy. The largest gratings at the time, 30 cm x 40 cm, were fabricated and integrated to the system. These first gratings were produced by Jobin-Yvon, now Horiba, with reflectivity of 90% and a damage threshold of 0.1 J/cm2 and proved sufficient for a convincing demonstration of high energy CPA.

With P102 retrofitted in CPA, we produced successfully 20 TW (Sauteret et al., 1991); and later 50 TW (Rouyer et al., 1993). Similar result few months later where obtained independently at ILE in Japan by Yamakawa et al. (1991). These results showed clearly that the CPA could work at any arbitrary energy level and would be capable to produce PW pulse. Indeed, as we predicted, the first Petawatt pulse was demonstrated by Perry et al. (1999), ten years after the first terawatt. One of the impressive hurdles overcome by Perry's group was the fabrication of meter-size diffraction gratings. They revolutionised the field.

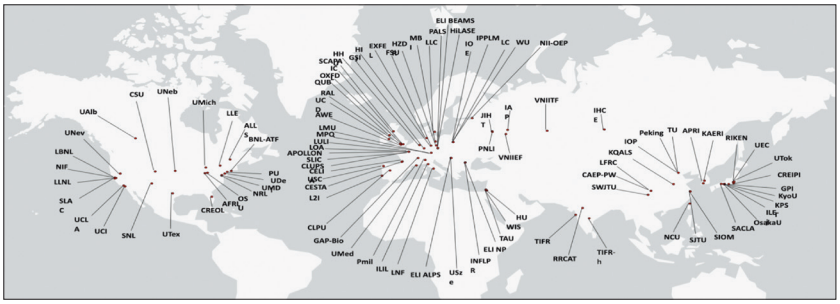

Figure 7. World map of lasers with peak power >100TW.

In parallel to the Nd:glass based petawatt systems, we have today a number of high-power Ti:sapphire-based systems. They exhibit much shorter pulses in the 20–30 fs range, and energies in the 5–10 J range, thus delivering peak power of 100 TW. A 100 TW class Ti:sapphire laser was first demonstrated at the University of California at San Diego (Barty et al., 1994). The leading laboratories at the present time in this area are CoReLS Research Center, in Korea, APRC in Japan with around 500 TW (Aoyama et al., 2002), Janus System at Lawrence Livermore, 200 TW, the Laboratoire d'Optique Appliquée (LOA) in France with 100 TW, the Max Born Institute in Germany with 100 TW, the Lund University in Sweden with 30 TW, and the Center for Ultrafast Optical Science University of Michigan with 200 TW. Today nearly one hundred 100 TW systems are operating (Fig. 7) with about 20 systems at the PW level (Fig. 8) existing or under construction. Groups in China (SIOM), Russia (APC), and the USA (LLE) are now aiming at the 100 PW level.

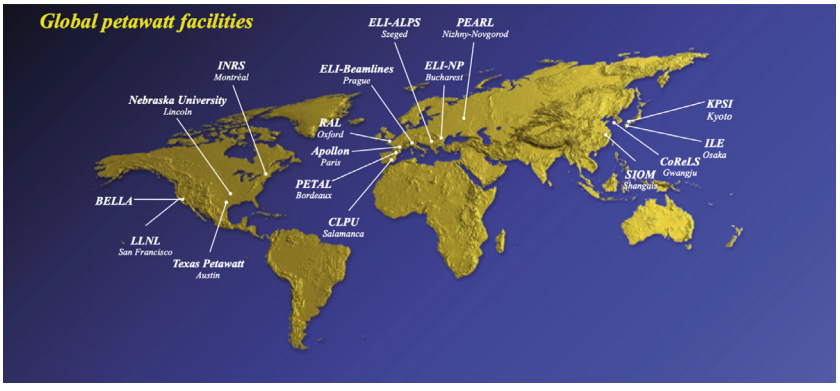

Figure 8. World map of lasers with peak power 1PW.

H. Optical Parametric Chirped Pulse Amplification (OPCPA)

In this section we discuss the differences between the CPA and OPCPA methods. Fig. 9 shows the conceptual layout of an Optical Parametric CPA, OPCPA system (Dubietis et al., 1992; Ross et al., 1997). Because we are reviewing only relativistic intensity laser we will not mention the large number of projects related to the sub-relativistic regime using OPCPA. As in CPA the objective in OPCPA is to stretch the pulse to a nanosecond duration and then amplify it to the joule or higher level by optical parametric amplification and recompress it back to close to its initial value. Note that the stretching is essential not only to keep the B integral low but also to pump and extract the energy efficiently. It is only during the stretched pulse that light can be transferred from the pump beam to the signal beam. Consequently, the pump pulse duration and that of the stretched pulse must be as equal as possible. The advantages of this technique are as follows:

1. Large bandwidth that could accommodate few-cycle pulses.
2. Ability to benefit from very large KDP crystals (100 × 100 cm2) developed for laser fusion.
3. Adaptability to existing laser fusion chains, which benefit from low-bandwidth well collimated nanosecond laser pulses at 532 nm.
4. No heat dissipation in the OPA crystal itself, this is important for high average power.
5. No transverse amplified stimulated emission, which is a major source of loss for large-aperture Ti:sapphire systems.
6. Ability to use an iodine laser as a pumping source.
7. Very simple amplification system.

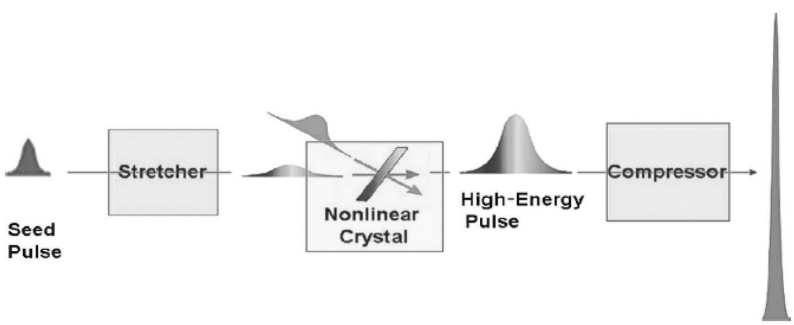

Figure 9. OPCPA concept. In the OPCPA the pulse is amplified by optical parametric amplification instead of regular optical amplification. Note that for efficiency the pump pulse and the stretched pulse must have approximately the same duration and the same spatial extend.

The disadvantages are as follows:

1. Lower efficiency than standard CPA. For a standard Ti:sapphire CPA, the efficiency can be as high as 50% from a long green pulse, say of 50 ns. The energy storage time of Ti:sapphire is 2 μs. So CPA is overall a more efficient system.
2. Very large stretching ratio, in the range of 10^6 to 1, i.e. 10 fs to 5 ns, necessary for energy extraction. This will make pulse compression down to the 10 fs regime difficult.
3. Gain is a significant function of the intensity. This means the pump-beam profile may affect the beam quality and needs a high level of control.

In both systems, the pulse duration will ultimately be limited by the grating bandwidth. At present no large gratings have the efficiency and the bandwidth necessary for efficient pulse compression much below 30 fs. Beam quality from CPA has been demonstrated to be excellent. The latest studies have shown that OPCPA can also provide good spatial beam quality (Collier et al., 1999). The potential of this technique has been demonstrated with the production of a 35 J, 85 fs pulse, equivalent to 0.4 PW, using a 10 cm-diameter beam (Collier et al., 2004). The possibility of reaching high energies seems to be more straight-forward with the OPCPA because it can benefit from kJ, ns fusion lasers that are already up and running. The pulse duration, however, will be limited by the grating bandwidth. CPA implementations must wait for large Ti:Sapphire crystals grown to 20×20 cm2 dimensions. These larger-scale crystals should become available as the demand for higher peak power increases.

III. BEYOND THE HORIZON: THE ZEPTOSECOND AND EXAWATT DOMAIN

In their pioneering experiment Grischkowsky and Ballant (1982) used a single mode optical fibre and were able to compress a picosecond pulse with nJ energy to the femtosecond level. This work triggered an enormous interest. To go higher in energy Orazio Svelto and his group (Nisoli et al., 1996) introduced a compression technique based on a fused silica hollow-core capillary, filled with noble gases to broaden the pulse spectrum before efficiently compressing to the 100 μJ level with chirped mirrors that introduce negative dispersion to the pulse phase. Refining this technique Orazio Svelto, Ferenc Krausz and collaborators (Nisoli et al., 1997) could compress a 20 fs into 5 fs or 2 cycles of light at 800 nm.

For higher energy, bulk compression was attempted by Rolland and Corkum (1988). In their implementation, the pulse is free-propagating in

a solid and not guided anymore. The pulse was relatively long, around 50 fs, with an input energy of 500 μJ leading to an output pulse of 100 μJ in 20 fs. However this scheme is impaired by the beam bell shape intensity distribution. This leads to variation in the nonlinear response across the beam profile and a corresponding variation of the compression factor.

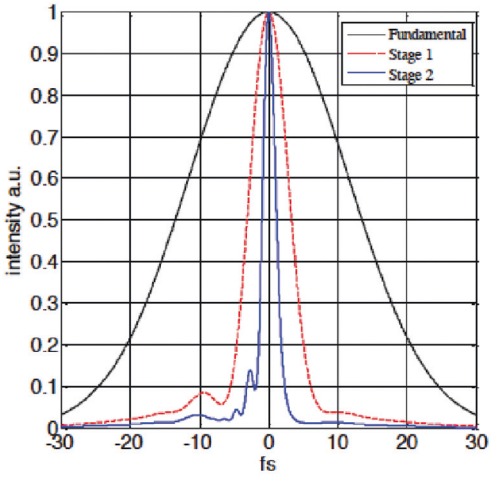

Figure 10. This element uses a uniform thickness plastic element of around .5mm. An incident flat top pulse will induce a uniform self-phase modulation across the element. After spectral broadening the pulse is compressed by 2 chirped mirrors to a near single cycle pulse into a 2.1 fs after two compression stages.

A. Large Energy Pulse Compression: Thin Film Compression (TFC)

Recently we have proposed a technique (Mourou et al., 2014) to compress 25 fs large energy pulses as high as 1 kJ to the 1–2 fs level. We call this approach the Thin Film Compressor, or TFC, and its principle is shown in Fig. 10. As shown in our simulation, this method is very efficient >50% and preserves the beam quality. Here the technique relies on the flat top nature of the high energy pulse and uses a thin "plastic" film of ~500 μm with a diameter of 20 cm. The element, that we call plastic for simplicity, will be transparent and exhibit a uniform thickness. The modelling of the pulse propagation leading to spectral broadening due to the nonlinear processes that occur within the film is described in Akhamov et al. (1992). After spectral broadening the pulse is compressed by chirped mirrors to a near single cycle pulse showing a pulse of 2.1 fs after two compression stages. This represents the shortest pulse duration that can be achieved based on the limitation defined by the laser wavelength, λ. Once the pulse is focused on λ^2 the pulse is in the desired λ^3 regime. The λ^3 regime is the focus volume that achieves the highest intensity for a given pulse energy. In order to increase the intensity, it is necessary to shift to shorter wavelengths that can support shorter pulse durations and tighter focusing.

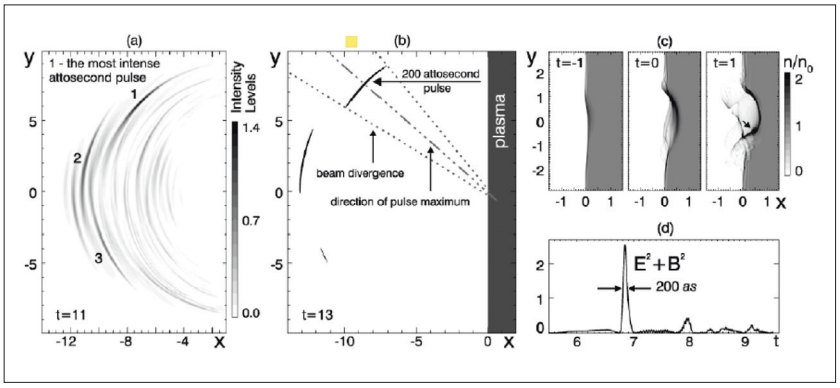

Figure 11. The pulse is focused on λ2 and create a mirror with an indentation deforms due to (a). As it moves relativistically, it provides an isolated an individual pulse (b), (c).

The proposed method for up-converting to shorter wavelengths is through a relativistic plasma mirror, and especially in the laser conditions of the λ^3 regime (Mourou et al., 2006). The relativistic mirror is not planar and rather deforms due to the indentation created Fig 11c by the focused Gaussian beam. As it moves relativistically in and out and sideways, the reflected beam is broadcast in specific directions and provide an isolated an individual pulse Fig. 11 a, b. In the relativistic regime (Naumova et al., 2004), predicts a pulse duration T compressed by the relativistic mirror-scaling like T = 600 [attosecond]/a_0. (Fig. 12) Here a_0 is the normalised vector potential, which is unity at 10^{18} W/cm^2 and scales as the square root of the intensity. For intensities on the order of 10^{22}–10^{24} W/cm^2 where a0 is on the order of 100 to 1 000, the compressed pulse could be only a few attoseconds, even zeptoseconds. Naumova et al. (2004) have simulated the generation of thin sheets of electrons of few nm thickness, much shorter than the laser period. It opens the prospect for X and gamma coherent scattering with good efficiency.

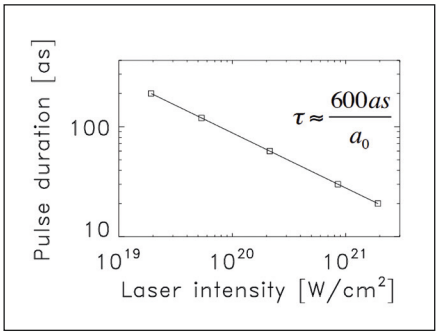

Figure 12. Naumova *et al.*, (2004) predicts a pulse duration scaling like *T*=600 (*attosecond*)/a_0.

IV. LASER PLASMA ELECTRON ACCELERATION

The concept of laser-plasma wake-field electron accelerator was proposed in 1979 by Toshiki Tajima and John M. Dawson (1979). In a laser-plasma accelerator (LPA), a plasma medium (e.g. fully stripped helium or hydrogen ions surrounded by free moving electrons) is used to transform electromagnetic energy from a laser pulse into kinetic energy of accelerated electrons by exciting high amplitude plasma density waves. See Fig. 13. An intense laser pulse (Esarey, 1996; Everett et. al., 1994; Clayton et. al., 1994; Umstadter et. al., 1996) causes the plasma electrons to move out of its path through the "photon pressure". The much heavier ions barely move and as a consequence are left unshielded. Some distance behind the laser pulse, the electrostatic force exerted by the ions on the electrons pulls them back to the axis, creating an electron density peak. The pattern of alternating positive and negative charges is referred to as a plasma wave or laser wake and supports an electric field. The wave oscillates at the plasma frequency which scales as the square root of the plasma density and has a wavelength typically around 10 to 100 μm. This is several orders of magnitude shorter than the typical RF period used in conventional accelerators. The amplitude of the plasma wave or strength of the electric field is proportional to the square root of the plasma density (number of free electrons per unit volume) and proportional to the laser intensity (for intensities $\geq 10^{18}$ W/cm^2). For typical densities (10^{18}–10^{19} electrons/cm^3) used in experiments, fields ranging from 10–100 GV/cm are produced, three orders of magnitude greater than with conventional technology. The wave's phase velocity is near the speed of light and electrons injected at the proper phase can be accelerated to high energies. To reach the same particle energy, plasma accelerators can then, in principle, be three orders of magnitude shorter than their conventional counterparts.

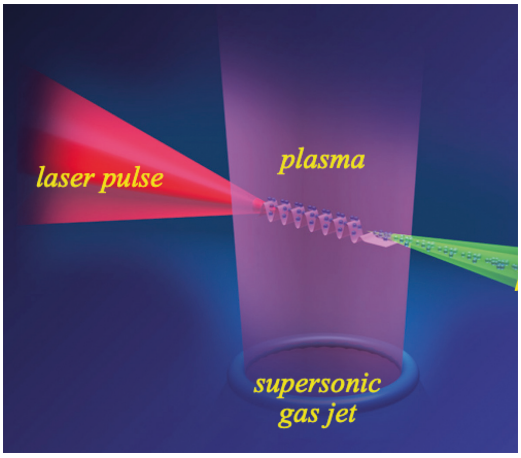

Figure 13. The Laser Wake Field Acceleration concept relies on the very large radiation pressure inducing a plasma wave. Electrons will be trapped in the wave and accelerated to energy of GeV/cm, a thousand time greater than conventional technology.

The wavelength of the plasma waves is also around three orders of magnitude smaller than the wavelength of the radiofrequency used in conventional accelerators. The generation of low energy dispersion electron bunches requires that the length of the bunch to be a small fraction of these wavelengths and/or the use of complex techniques only compatible with a large facility. In the case of plasma accelerators this condition implies the use of electron bunches shorter than 10 fs to get an energy dispersion below 10% typically. So far, these short pulses were produced by controlling the wavebreaking of the plasma waves or by using laser beam collision in the acceleration zone to produce a strongly localised injection. In a relatively short time the major hurdles, one after the other, have been surmounted.

Considering the beam monochromaticity, it has been simultaneously demonstrated (Mangles et. al., 2004; Geddes et. al., 2004; Faure et. al., 2004) to be of the order of 1%. In addition, high energy electrons have also been shown to the GeV level by several groups in the USA at the Lawrence Berkeley Laboratory, the Texas Petawatt Facility, University of Texas; in Korea at CoReLS; and in China at SIOM and Peking University.

That considered, the major stumbling blocks to laser-based acceleration (the repetition rate, average power and poor efficiency) due to the inherent low repetition rate of the driving laser are being addressed. Revolutionary laser infrastructures based on phased-array-optical fibre, like the Coherent Amplification Network (CAN) described in section II. F. are being actively studied. (Mourou et al., 2013)

Accelerator technology has immense promise for innovation for various applications ranging from science with High Energy Particle Physics, to applications which include betatron and free-electron light sources for diagnostics or radiation therapy and proton source for hadron therapy as well as homeland security.

V. HIGH ENERGY PROTON BEAMS, PROTON THERAPY

It has been shown that laser thin-target interactions can produce plentiful MeV protons in a beam with superior transverse emittance. The proton generation is a direct consequence of electron acceleration. Electrons that are violently accelerated in the laser field can draw behind them protons that are on either the front or back surface of the target.

Highly energetic proton beams have been demonstrated at Livermore, LULI, CUOS, and Rutherford with intensities of 10^{18}–10^{20} W/cm^2. They could lead to important applications such as fast ignition for inertial confinement fusion as was pointed out by Roth et al. (2001) and proton therapy (Bulanov and Khoroshkov, 2002; Fourkal et al., 2002).

The proton used in radiotherapy and oncology provides several advan-

tages. First, proton beam scattering on atomic electrons is weak and results in low irradiation of healthy tissues surrounding the tumour. Second, the stopping length for the proton with a given energy is fixed and avoids irradiation of the healthy tissues at the rear side of the tumour. Third, the Bragg peak of the energy losses provides substantial energy deposition in the vicinity of the proton stopping point.

Currently, proton beams with the required parameters are produced with conventional charged particle accelerators: synchrotron, cyclotron, and linear accelerators. The use of the laser accelerator is very attractive because its compactness is associated with additional possibilities for controlling proton beam parameters. The typical energy spectrum of laser-accelerated particles observed both in experiments and in computer simulations can be approximated by a quasi-thermal distribution with a cut-off at a maximum energy.

The effective temperature attributed to fast ion beams is within only a factor of a few from the maximum value of the particle energy. On the other hand, the above-mentioned applications require high-quality proton beams, i.e. beams with sufficiently small energy spread $\Delta E / E$. For example, for hadron therapy it is highly desirable to have a proton beam with $\Delta E / E = 2\%$ in order to provide the conditions for a high irradiation dose being delivered to the tumour while sparing neighbouring tissues.

In the case of the ion injector, a high-quality beam is needed in order to inject the charged particles into the optimal accelerating phase. Bulanov and Khoroshkov (2002) have shown that such a beam of laser-accelerated ions can be obtained by using a double-layer target. Multilayer targets have been used for a long time in order to increase the efficiency of the laser energy conversion into plasma and fast particle kinetic energy; see, for example, Badziak et al. (2001, 2003). In contrast to the previously discussed configurations, the use of a double-layer target was proposed in order to produce fast proton beams with controlled quality. In this scheme the target is made of two layers with ions of different electric charge and mass.

A regime of ion acceleration that exhibits very favourable properties has been identified by Esirkepov et al. (2004). In this regime the radiation pressure of the electromagnetic wave plays a dominant role in the interaction of an ultra-intense laser pulse with a foil. In this radiation pressure dominant regime, ion acceleration appears due to the radiation pressure of the laser light on the electron component with momentum transferred to ions through the electric field arising from charge separation. In this regime, the proton component moves forward with almost the same velocity as the average longitudinal velocity of the electron component. Thus, the proton kinetic energy is well above that of the electron component. In addition, in the radiation pressure dominant regime the ion accel-

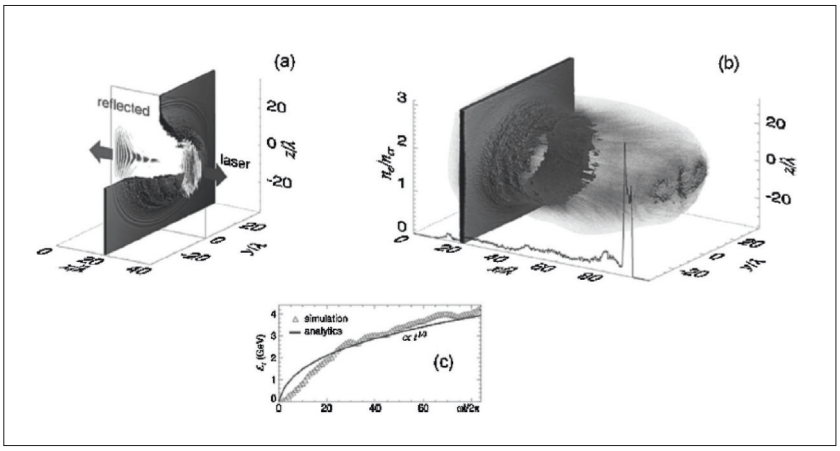

Figure 14. In this regime for intensity in the 1023 W/cm2, the radiation pressure is dominant and scales with the laser-pulse energy.

eration mechanism is found to be highly efficient, and, as we shall explicitly show, the ion energy per nucleon is proportional to the laser-pulse energy. The main results of three-dimensional PIC simulations are shown in Fig.14.

A. Proton acceleration in the single-cycle regime

Single-Cycled Laser Acceleration (SCLA) of ions (Zhou et al., 2016) relies on laser pulses which give access to a new ion acceleration regime. Historically, attempts in laser acceleration of ions relied on the multi-cycle, high-energy pulses available. The first experimentally realised laser ion acceleration was TNSA (Cousens et al., 2006). In this mechanism the target was thick, electrons penetrated through the thick target and ions were not adiabatically trapped and accelerated. Rather ions were accelerated on the surface of the fixed target over the sheath. For the foil thickness l we define the normalised electron areal density $\sigma = n_e\, l/n_c\, \lambda$ as the target parameter. One way to increase the adiabaticity and prolong the interaction for ion acceleration was to reduce the mass of the target. This reduced σ, as in the regime of Coherent Acceleration of Ions by Lasers (CAIL) (Yan et al., 2010) is far different from the TNSA regime. Radiation Pressure Acceleration (RPA) (Esirkepov, et al., 2004) increases a_0 and slightly decreases σ as compared with TNSA. SCLA, by the virtue of the decreased pulse length of the laser, also reduces σ and increases a_0. Thus, due to the reduction in σ and increase in a_0 for SCLA (and RPA) relative to TNSA, the coherence of the ion acceleration is enhanced. Two clear advantages then arise with SCLA over the longer pulse driven RPA: first,

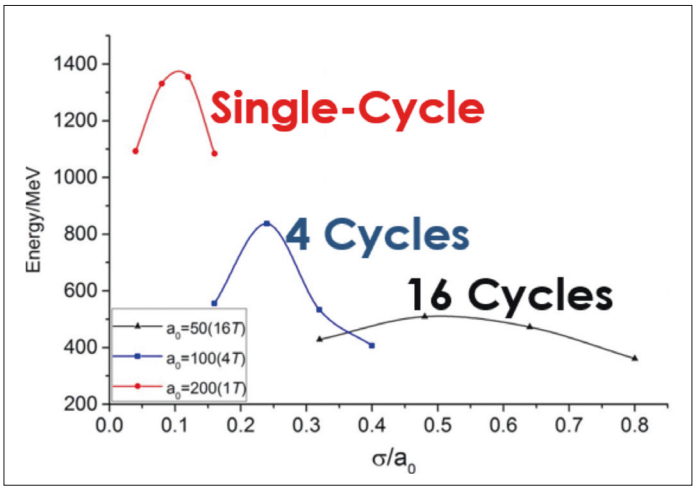

Figure 15. In the single-cycle regime, the acceleration efficiency of ions varies sharply. The fewer number of cycles translates into a larger laser vector potential and yields higher proton cut-off energy. The proton energy is increased by reducing the number of cycles from $\tau = 16T$ (black curve) where T is the period, to $\tau = 4T$ (blue curve). In particular, with the single-cycle pulse (red curve), the cut-off energy of the ions is increased by a significant amount and becomes quickly relativistic.

the pulse intensity is enhanced for a given laser energy as the pulse duration is reduced; second, the elimination of multi-cycle averaging over the oscillations of a longer pulse enhances the efficiency, coherence, and stability of the ponderomotive acceleration. See Fig. 15. With this combination, the ion acceleration in the limit of single-cycle laser pulses becomes far more robust, stable and intense due to the simple fact that the electron ponderomotive acceleration term ‹v×B› no longer requires cycle-averaging as in the case of longer, multi-cycle pulses. The application of the single-cycle regime introduces a more coherent electron acceleration and sharper electron layer formation that creates the fields that will ultimately accelerate the trailing ions.

We know that in an ideal RPA light sail regime, the resultant maximum ion energy is inversely proportional to the total mass of the accelerated target. In a simple picture, the optimum thickness is achieved by decreasing it, namely, the lower the total mass, the higher the final maximum energy. However, other physical processes, such as transverse instabilities, will strongly affect the actual acceleration process and prevent it from reaching the optimum acceleration, particularly with current state-of-the art multi-cycle ultra-intense laser pulses. While for shorter pulse durations, especially for single-cycle pulses, the duration is too short for

those instabilities to develop and the constraints caused by instabilities are strongly suppressed, which gives us more opportunity to approach to the ideal case. So compared to the traditional RPA, the optimal target thickness becomes smaller. Specifically, SCLA is located within the transparent area ($\sigma << a_0$) corresponding to smaller values for $\sigma_{opt.}$

VI. NEUTRON SOURCES

Neutron beamlines produced by CPA will enable a broad range of both fundamental and applied science. Thermal neutron sources (~meV–eV) are widely used for diffraction and spectroscopy experiments (Blomgren et al., 2006). and fast neutrons (~MeV) can be applied to radiography, medicine and material damage studies (Rynes et al., 1999). Laser generated sources of neutrons hold the advantages of a small source size and pulse duration and synchronicity with other secondary sources. Imaging using combined sources can yield information about the composition of materials. The intense source of γ-radiation planned at ELI-NP, for instance, also opens up the possibility of a revolutionary thermal neutron source generated through neutron halo isomers. This scheme avoids the need for moderation of the neutron energy and is predicted to generate neutron fluxes orders of magnitude higher than at existing spallation sources (Habs et. al., 2010).

A. Laser based sources

Laser-driven neutron sources are based on DD or DT fusion and (p,n) and (γ,n) reactions. There are two approaches: reactions between ions within a single laser-heated deuterium target or conversion in a secondary target of a laser driven ion or γ ray beam.

B. Single target scheme

Neutrons can be generated by irradiating thick solid deuterated plastic targets with intense lasers. A series of experiments with 1–100 TW lasers demonstrated yields up to 10^7–10^8 n sr^{-1} per shot (Pretzler et al., 1998; Izumi et al., 2002). Highly energetic deuterons heated directly by the laser at the front surface stream into the target and so initiate ‘beam-target’ fusion reactions with cold deuterons within the bulk of the solid. The angular distribution of the neutrons is closely related to that of the accelerated ions and is predominantly in the forward direction for short scale-length plasmas. Particle-in-cell code modelling of this mechanism is in good agreement with these experimental results and identified laser and plasma parameters, which lead to the production of an energy tuneable,

quasi-mono-energetic forward-directed fast neutron beam. Fusion reactions can also be initiated in gases or a mist of sub-micron droplets produced using pulsed gas jets. The presence of solid-density clusters or droplets dramatically increases the absorption efficiency of short pulse intense irradiation, which can exceed 90% of a petawatt-class laser pulse (Gumbrell et al., 2008). Because the interaction is with an extended target several millimetres in length, 'beam–beam' reactions can occur between hot deuterons within the plasma as well as 'beam–target' reactions with the surrounding medium. If the emission is dominated by the thermonuclear process, then the duration of the neutron burst is limited to less than a nanosecond because the ions rapidly traverse the laser-heated volume. These experiments have been performed using D_2, CD_4 or D_2O and in principle can use a mixture of the tritiated forms of these materials. These sources are generally considered as isotropic, with their flux scaling strongly with the laser energy.

C. Double target scheme

In 'pitcher-catcher' experiments a primary target (pitcher) is irradiated with an intense laser pulse to generate an ion beam from the rear surface. The catcher is a slab of material which acts as a neutron converter in the same way as they are used on accelerator facility neutron sources. DD fusion in deuterated plastic catcher targets yielding ~10^4 neutrons per shot has been demonstrated using liquid droplets as the laser interaction target (20 μm diameter D_2O), enabling a high repetition rate.

The same arrangement can employ the large fluxes of γ rays produced in intense laser plasma interactions to initiate (γ,n) reactions in the catcher sample. These photo-neutrons are usually measured to diagnose the interaction rather than being optimised to investigate their potential as a source and so yields tend to be low (~100 neutrons per shot). In the next section we discuss a preferable option for generating neutrons using γ beams.

D. Neutron spallation

High intensity lasers can produce high energy protons in the several 100 MeV regime. These can be used to strike a target of a heavy metal, mercury or tantalum. Each impact can produce 20–30 high energy neutrons per spallation. This technique has the advantage of producing a beam of neutrons that can be modulated. This process may be linked to conventional nuclear reactor technology in an accelerator-driven system (ADS) to transmute long-lived radioisotopes in used nuclear fuel into shorter-lived fission products.

VII. X-RAYS

Since the dawn of the laser in 1960, scientists focused them to create non-linear effects and very quickly, as intensity increased, plasmas. Plasmas are ionised media known before the existence of lasers to be good emitters of X-rays. Naturally, laser-driven plasmas were studied for the generation of incoherent as well as coherent X-rays. The first proposal of a laser emitting X-rays was published in 1967 by Duguay and Rentzepis (1967), only seven years after the demonstration of the first ruby laser by Theodore Maiman. However, progress on the development of both incoherent and coherent X-rays was slow following delays in the evolution of the laser intensity. The demonstration and then the implementation of the CPA technique triggered a major change of paradigm for the field of laser-driven X-ray sources. This section gives a short overview of the different X-ray sources generated by laser that are available today with special attention on the impact of CPA technique.

A. Incoherent X-ray sources:

By focusing an intense laser on a gaseous, liquid or solid target, plasma is created that emits X-rays through Bremsstrahlung or after atomic inner shell excitation (K-α emission) of the cold solid part of the target. To be able to excite inner-shells, the electron kinetic energy has to be higher than the atomic level energy. Prior to CPA, acceleration of electrons inside the plasma was just sufficient to produce K-α emission from low atomic number elements like Aluminium (1.48 keV) and Copper (8 keV). The jump in intensity provided by CPA induced very strong electron acceleration in the plasma leading today to the production of K-α from elements as heavy as Gold (68.8 keV). Furthermore, in these conditions, Bremsstrahlung emission has been observed to extend up to several 100's of keV. Experiments have also used external laser-accelerated electron beams with energy up to several 100's of MeV leading to Bremsstrahlung emission extending also to 100's of MeV. All these developments are of high interest for medicine (radiotherapy or imaging) and for non-destructive imaging.

B. Coherent X-ray sources:

The interaction of an intense picosecond or femtosecond laser with a gas may generate the odd harmonics of the fundamental laser with a spectrum extending to a cut-off limit given by the law $Ec \approx 3.12\ U_p + I_p$ where Ip is the ionisation potential and $U_p = I\ \lambda^2$ and λ being the fundamental laser wavelength. It is apparent that by increasing the intensity, CPA allowed an extension the cut-off to much higher photon energies,

although only up to a saturation point. Today multi-keV high harmonics have been demonstrated using a 4 μm CPA laser. Moreover, gas ionisation is detrimental for the phase-matching between the infrared laser and the high harmonics, thus limiting the energy transfer between them. Using ultrafast (the best being single-cycle) and intense laser pulses ensures strong high harmonic emission. High harmonics having their spectral phase locked demonstrate the emission of attosecond duration pulses. Last but not least, high harmonics maintain the optical properties of the fundamental laser: their wavefront might partially be controlled by the IR laser wavefront (Gauthier et al., 2008), their angle of polarisation is following that of the IR laser (Vodungbo et al., 2011) and they are very coherent. They are thus excellent X-ray sources for fundamental and societal applications.

High harmonics might be also produced by the interaction of a very intense laser (10^{19} W cm^{-2} and above) with solid target. In that case, the laser excites the electron from the target surface, pushing and pulling them away every half cycle. Therefore the electrons generate a train of attosecond X-ray bursts (Teubner and Gibbon, 2008). In some extreme cases, the laser can be back reflected by the relativistic electrons expelled from the surface. The laser is Doppler shifted to much higher photon energies, reaching the keV range. The pulse is also compressed down to 100's of attoseconds or shorter (Naumova et al., 2004; Tsakiris et al., 2006). The X-ray source is highly coherent and controllable by adjusting the laser and target parameters.

It is well-known that at high intensities, the interaction of a CPA laser with gas accelerates electrons up to 100's MeV and even at a few GeV over few millimetres of gas. Such high acceleration gradient is achieved in the so-called "bubble regime" where the laser pushed away the electrons from its path, leaving on its back a bubble with a deficit of electrons and thus an excess of ions. The expelled electrons can thus be accelerated inside this bubble due to the high electric field while for some conditions they also start to oscillate transversely producing betatron oscillations. This source emits radiation with a cone aperture varying as $1/\gamma^2$, γ being the Lorentz factor. The radiation is a "white spectrum" with a cut-off energy depending on γ^2. With a 100 TW-class laser, emission up to 20 keV has been demonstrated within a cone of a few degrees. The emission intrinsically has the duration of the laser (few fs) and the size of the focal spot (few μm) making for a very promising source for medical applications as well as for imaging.

As mentioned above, in the late 60s–early 70s research proposed different schemes for producing a real X-ray laser i.e. by creating a population inversion in plasma necessary for stimulated amplification of spontaneous emission (ASE). Although researchers were very active using non-

CPA lasers and saturated amplification was demonstrated in 1991, the emergence of CPA created a revolution. Thanks to CPA and the possibility of achieving ultra-high intensity, the energy of the pump laser was quickly reduced from kJ, to 10's of J and later joules with a subsequent jump in repetition rate from 10^{-4} Hz to 10 Hz. It is worth noting that the ASE regime without a cavity (normal X-ray mirrors are not suitable for a cavity) led to weakly coherent X-ray lasers. By seeding the amplifying plasma with fully coherent high harmonics produced by the interaction of a CPA laser with gas, the amplified beam is demonstrated to be fully coherent, polarised (either linear or circular depending of the incoming beam) (Zeitoun et al., 2004) and having an excellent wavefront (Godet et al., 2009).

C. X-ray CPA

Recently, it was proposed to use the CPA technique directly in the X-ray range for both free-electron lasers (FEL) and plasma-based X-ray lasers (PBXRL). Although the physics behind the X-ray amplification in FEL and PBXRL is different, the general concept is very similar: While amplifying an ultrashort X-ray pulse, typically femtosecond, most of the energy stored in the medium is left untouched because of a temporal mismatch (Wang et al., 2014; Oliva et al., 2012). By stretching the incoming femtosecond X-ray pulse, then amplifying and finally compressing the pulse, most of the stored energy may be transferred to the X-ray pulse. The concept was successfully demonstrated on an FEL (Gauthier et al., 2016).

Thanks to the CPA these sources are now mature and used for applications in various domains from biology, chemistry and physics.

VIII. ATTOSECOND SCIENCE

Attosecond science represents one of the frontiers in Ultrafast Optics, since it offers the possibility to initiate and control the motion of electronic wave packets inside atoms, molecules, nanostructures and solids. It is now a well-established research field, which offers formidable tools for the investigation of fundamental electronic processes (Calegari et al., 2016).

The production of attosecond pulses is based on high-order harmonic generation (HHG) in gases, which is a highly nonlinear process taking place when an intense (10^{13}–10^{15} W/cm^2) and short laser pulse is focused into a gas medium. The HHG process then results in the production of coherent extreme ultraviolet (XUV) radiation with pulse duration down to the attosecond regime. The physical processes giving rise to HHG can be understood in the framework of a quasi-classical three-step model (Schafer et al., 1993; Corkum et al., 1993). According to this model the

most weakly bound electron tunnels through the energy barrier formed by the Coulomb field in the presence of the driving electric field. It then accelerates in the oscillating field as a free particle to eventually recombine with the parent ion, thus emitting a high energy photon. This process is periodically repeated every half optical cycle of the fundamental radiation, thus leading to a periodic emission of very short radiation bursts, with duration in the attosecond range, as first experimentally demonstrated by Paul et al. (2001).

For a number of important applications, such as pump–probe experiments, it is essential to isolate a single pulse of the train, which can then be synchronised with another optical pulse (Sansone et al., 2010a). The first experimental demonstration of isolated attosecond pulses was reported by Hentschel et al. (2001). A few developments in femtosecond laser technology were essential to achieve the generation of isolated attosecond pulses, in particular the stabilisation of the carrier-envelope phase (CEP) of the driving pulses (Jones et al., 2000) and the generation of high-peak-power sub-5-fs pulses (Baltuška et al., 2003). The most common way to generate high-peak power, few-optical-cycle pulses is to apply suitable post-compression schemes. The most common technique is based on spectral broadening in hollow fibres filled with noble gases, in combination with broadband dispersive delay-line with chirped mirrors (Nisoli et al., 1996, 1997).

Attosecond pulses were first employed for the investigation of ultrafast electron dynamics in atomic physics. Particularly interesting is the measurement of the delay in photoemission (Schultze et al., 2010; Klünder et al., 2011), the analysis of the process of tunnel ionization (Dudovich et al., 2006; Uiberacker et al., 2007), the investigation of electronic correlation in helium (Ossiander et al., 2017) to name but a few examples. The first application of attosecond pulses to molecular physics was reported in 2010, with the measurement of the electron localisation process in H2 and D2 molecules after ionisation induced by isolated attosecond pulses (Sansone et al., 2010b). By employing high harmonic spectroscopy, attosecond charge migration was measured and controlled in ionised iodoacetylene by analysing the harmonic light emitted after excitation of the neutral molecule with a strong NIR pulse (Kraus et al., 2015). Particularly interesting is the possibility to investigate the ultrafast electron dynamics in complex molecules where sudden ionisation by attosecond pulses may produce ultrafast charge migration along the molecular skeleton induce a nuclear rearrangement (Cederbaum et al., 1999; Remacle et al., 2006). The process of electron transfer in molecular complexes is of crucial importance in biochemistry since it triggers the first steps in a number of biochemical processes, such as photosynthesis and electron transport along DNA. Experimental evidence of charge migration initiated by iso-

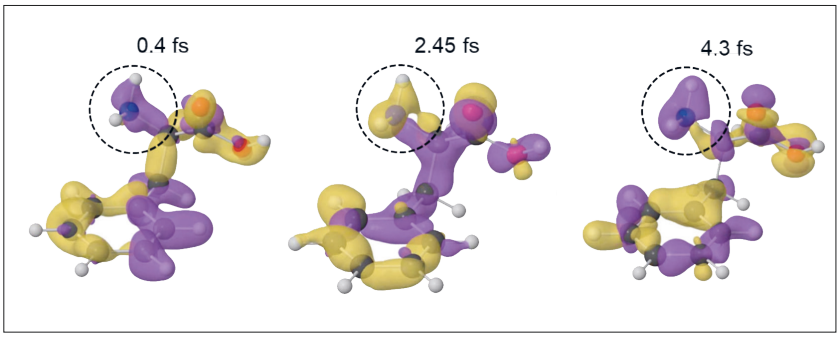

Figure 16. Electron density around the amine group of phenylalanine changes sign in ~2 fs.

lated attosecond pulses were first reported in 2014 in the amino acid phenylalanine- (Calegari et al., 2014). Charge migration was evidenced as an oscillatory evolution in the yield of a doubly-charged molecular fragment. Fig. 16 shows the calculated temporal evolution of the electronic wave packet generated by the attosecond pulses.

Attosecond technology has also been employed to study ultrafast processes in condensed matter. The first application of attosecond pulses to solids was reported in 2007, with the observation that photoelectrons from the 4f band of tungsten reach the surface ~100 attoseconds later than those from the Fermi-edge (Calegari et al., 2014). Another very interesting application was reported in 2013, with the observation of an insulator-to-conductor transition in fused silica (Schultze et al., 2013). It was demonstrated that the ac conductivity of fused silica can be increased by more than 18 orders of magnitude, within 1 fs, by using few-optical-cycle NIR pulses (Schiffrin et al., 2013). The process of tunnel ionisation has been investigated in solids by measuring the transmission of isolated attosecond pulses through a single-crystalline, free-standing Si membrane as a function of the delay with respect to a NIR pump pulse, which excites electrons from the valence band to the conduction band (Schultze et al., 2014). A photo-assisted tunnelling injection mechanism called the dynamical Franz-Keldysh effect has been observed in thin films of polycrystalline diamond (Lucchini et al., 2016). This effect is based on electronic intra-band motion, which competes with inter-band transitions. More recently, the role of inter- and intra-band dynamics in electron transfer between valence and conduction bands in GaAs monocrystalline samples has been investigated by employing attosecond pulses (Schlaepfer et al., 2018).

IX. ASTROPHYSICS

Over the last decade, ion acceleration driven by ultra-intense laser pulses has been emerging as a very exciting potential alternative to conventional acceleration technology. By offering radically new characteristics (Fuchs et al., 2006; Macchi et al., 2013), such as extremely compact acceleration (over less than 1 mm), ultra-short (less than 1 ps) and ultra-dense bunches (over 10^{13} particles/bunch in a single shot), laser ion acceleration offers very promising applications as in hadron therapy and for the production of medical radioisotopes. But already, laser-accelerated ions are used in ground-breaking applications in proton radiography (Chen et al., 2012), to study the concept of rapid ignition for Inertial Confinement Fusion (Roth et al., 2001), and in the so-called field of "laboratory astrophysics" (Remington et al., 1999; Albertazzi et al., 2014; Gregori et al., 2012).

A new emerging prospect in this laboratory astrophysics domain (Chen et al., 2018) is to investigate the question of the nucleosynthesis of heavy elements. At present, there is no complete physical scenario capable of explaining and reproducing the observed abundances of super-heavy elements in our Solar System as well as in other systems (Arnould et al., 2007; Thielemann et al., 2011; Reifarth et al., 2014). These super-heavy elements (i.e. roughly half of the elements heavier than Iron, and almost all of those beyond Bismuth) are postulated to be generated through the r-process (Arnould et al., 2007). This process proceeds through multiple neutron capture in a nucleus, rapidly increasing its mass number (A) until a β^--decay (emission of an electron and a anti-neutrino) takes place, which leads to an increase in atomic number (Z). It is generally accepted that this process can occur only under extremely high neutron flux of more than 10^{20} n/[cm^2.s] (Cowan et al., 1985) in order for multiple neutron captures to take place despite the small cross-sections involved. The main problem is that almost all of our knowledge relative to the dynamics of the r-process rests on theory and simulations, but their accuracy is hindered by large uncertainties (Mumpower et al., 2016; Panov, 2016) in the nuclear data for the involved heavy nuclei (e.g. neutron capture rates, β-decay and α-decay half-lives, masses). This is due to the fact that no facility based on conventional technology- can even come close to such an extreme neutron flux.

To reverse this, ultra-intense lasers offer a radically new prospect as they could be used to generate ultra-bright neutron beams in order to make direct measurements of neutron capture, i.e. (n,γ) nuclear reactions, as well as subsequent β-decay rates of the radioactive isotopes that are created by the neutron capture (Chen et al., 2018). For this, the required short duration and high neutron flux could be generated, from laser-accelerated protons, through spallation. Another advantage offered by

ultra-intense laser facilities for such investigations is that they are equipped with auxiliary high-energy laser pulses, i.e. offering the possibility to perform nuclear measurements in a hot plasma environment that emulates astrophysical conditions.

To generate the required ultra-bright neutron beams through spallation, imminent multi-PW lasers offer the prospect of pushing the focused intensity of the laser beam on target by at least one order of magnitude compared to current lasers, i.e. to 10^{22} W.cm^{-2}, and even further, to 10^{23} W.cm^{-2}, with the help of refocusing plasma optics, allowing a reduction in the laser focal spot and a boost to the focused intensity (Nakatsutsumi et al. 2010, 2018). The immediate consequence should be to increase the maximum energy of the produced protons. Most notably, the domain above 200 MeV of maximum energy should be attainable (Chen et al., 2018), thus making it possible to significantly increase the throughput of neutron production by spallation. Spallation is a process that occurs when a light projectile (proton, neutron, or light ions) with a kinetic energy from several hundreds of MeV to several GeV, interacts with a heavy nucleus (e.g., lead) and causes the emission of a large number of hadrons (mostly neutrons) (Van der Meer et al., 2004).

Overall, multi-PW facilities like Apollon or ELI-NP can expect to produce >10^{12} neutrons from the protons in the output of a Pb converter. Using a conservative estimate of 50% for the proton beam bandwidth, it will debunch over ~0.7 ns after 50 cm, i.e. by the time it reaches the Pb spallation converter. Taking this as the duration of the neutron bunch (as the individual spallation process takes place over a ~10^{-22} s time-scale), and a source size imposed by the protons scattering in the Pb target (over 3 mm radius for protons at 250 MeV and 0.5 mm at 1 GeV), the conservatively estimated resulting peak flux will be ~10^{22}–5x10^{23} neutrons/[cm^2.s].

Also, because the repetition rate of the multi-PW lasers will be improved compared to present-day lasers, the time-averaged neutron flux should also become quite high. Using a repetition rate of 1 shot/min (for the largest facilities), the time-averaged flux neutron should reach ~1011–5x10^{12} neutrons/[cm^2.s]. This will greatly exceed those available on existing facilities and should permit multiple neutron capture (Couture and Reifarth, 2007).

We also note that such extreme brightness neutron sources will have a broad collateral effect aside from the nucleosynthesis application discussed here. Indeed, they could help satisfy the increasing demand for neutron sources (Hamm, 2010), e.g. for radioisotope production and even for more futuristic transmutation applications.

X. EXTREME LIGHT PROPAGATION IN QUANTUM VACUUM

Particle production in "empty" space is a historical path which has guided the field of Extreme Light with the ultimate goal of investigating laser-matter interactions in the new regime of ultra-relativistic optics reaching into the fundamental QED and possibly QCD regimes. The laser must necessarily be between the Petawatt and Exawatt regime to produce synchronised, high energy radiation and particle beams with extremely short time structures in the attosecond and zeptosecond time domain. These unique characteristics, unattainable by any other means, could be combined to offer a new paradigm to the exploration of the structure of a vacuum to respond to one of the most fundamental questions: how can light propagate in a vacuum; how can a vacuum define the speed of light; and how can it define the mass of all elementary particles?

A. Light propagation in a vacuum

The vacuum structure defines, for example, how light propagates, as first noted by Werner Heisenberg and his collaborators. The quantum fluctuations in the vacuum allow light-light scattering and the conversion of electromagnetic field energy into particle and antiparticle pairs. In particular, a photon traveling in the vacuum can fluctuate into a particle-antiparticle pair that is virtual because the energy of a single light photon is much smaller than that of a material particle pair. This transmutation of a photon into a virtual pair and back, is called vacuum polarisation since this process also alters the nature of the Coulomb law at short distance. If a second photon arrives just when the first photon exists in its electron-positron pair state, it can scatter from this virtual charged particle pair. In this way, light scatters from light. In direct extension of this argument, a strong electromagnetic field applied in the vacuum can deflect the virtual electrons and positrons. Therefore, there is an index of refraction of empty space filled with fields. In principle, light can be bent by applied electro-magnetic fields, just as gravity bends light through the deformation of space-time geometry. In this sense, empty space has a structure not all that different from that of a dilute gas. Because the Compton wavelength of an electron, h/mc = 386 fm (fermi = femtometer = one in 10^{15} part of a metre, the radius of a proton) is 3 million times shorter than a typical optical wavelength, vacuum structure does not massively obstruct the propagation of light. However, light propagating in the Universe over cosmological distances, in the presence of external magnetic fields experiences nonlinear vacuum effects such as photon splitting. It is important to recall that more than 50 years ago Julian Schwinger showed that a coherent ideal 'plane light wave' cannot scatter from

itself, or be influenced by itself, no matter what the field intensity is. This is the only form of light known to which the vacuum is exactly transparent.

B. Electromagnetic field in a vacuum

The gap between the valence and conduction band of the best insulator, the vacuum, is twice the energy equivalent of the electron mass, $V_0 = 2mc^2/e = 10^6$ volts. Such high potential differences are commonly achieved in specialised nuclear accelerators (Tandems, Van der Graaff), however over a rather large distance. The vacuum does not begin to spark since the electron-positron pair must materialise on two ends of the potential well, and this is for laboratory devices a macroscopic distance apart. The electric field strength controls the speed of vacuum sparking. The field strength for which this vacuum decay occurs at the zeptosecond scale (light travels a distance of the Compton wavelength $\lambda_c = 10^{-12}$ m in 10 zeptoseconds) is the so called 'Schwinger' critical strength E_0 (named after Schwinger, though Heisenberg was well aware of the result) for which the potential step V_0 occurs over the electron's Compton wavelength, that is $E_0 = 1.3\times10^{18}$ V/m. Approach to this field strength is the intermediate term goal of ELI. This corresponds to an intensity $I_0 = 4.65\times10^{29}$ W.cm^{-2}. One speaks also of laser power when the intensity within the typical focal domain of 1 μm^2 is considered; this value is $P_0 = 4.65\times10^{21}$ W, that is 4650 EW (E = exa = 10^{18}) or 4.6 zettawatt.

For fields near the Schwinger value E0 we can observe massive materialisation of pairs for fields existing at time scales of fs to as. The materialisation of electrical fields into electron-positron pairs is a diagnostic tool allowing for understanding how well the energy is focused. The abundant formation of electron-positron pairs is the first of many vacuum effects to study while striving to focus the laser energy into smaller and smaller volumes.

The stability of the vacuum described above has been studied and evaluated at absolute zero temperature. At finite temperature the valence-conduction particle-hole excitation, here pair production, can be induced. The temperature has a significant effect on vacuum stability, which for the attosecond time scale corresponds to the mass of an electron, $k T_e = mc^2$. Still, already at a fraction of this value massive thermally assisted vacuum decay will be encountered. There are many other ways which are currently discussed to bridge the 1–2 orders of magnitude in the field strength associated with the ELI or IZEST project, such as the Lorentz boost experienced by the electromagnetic field colliding with an electron beam.

XI. EXTREME LIGHT AS A BLACK HOLE SIMULATOR

Extreme light offers the promise to create a "tabletop" black hole. It could help to prove whether information is truly lost when black holes evaporate. The idea that information could be lost this way has created a paradox in our current understanding of basic physics.

The debate over whether information is really lost during what is called Hawking evaporation (see Fig. 17) has persisted in the 40 years since Stephen Hawking combined quantum field theory with Einstein's theory of general relativity and discovered black hole evaporation. Almost all contemporary leading theoretical physicists have participated in this "black hole war". In quantum mechanics, the probability, or information, must be preserved before and after a physical process. The seeming loss of information as a result of the evaporation of a black hole therefore implies that general relativity and quantum mechanics, the two pillars of modern physics, may be in conflict.

So far investigations of this paradox have been mostly theoretical because of the difficulty of observing black holes in their later stages, when this potential contradiction is most acute. According to theory, a solar-size black hole would take 10^{67} to evaporate entirely, yet our universe is only about 10^{10} years old. Therefore, essentially all astrophysical black holes are too young to provide useful clues on the information loss paradox even if they are observed, such as that responsible for the gravitational waves observed by LIGO in 2016.

Recently a laboratory black hole to simulate this evaporation has been conceived (Chen and Mourou, 2017). Using state-of-the-art laser and nanofabrication technologies, it is projected to mimic black hole evolu-

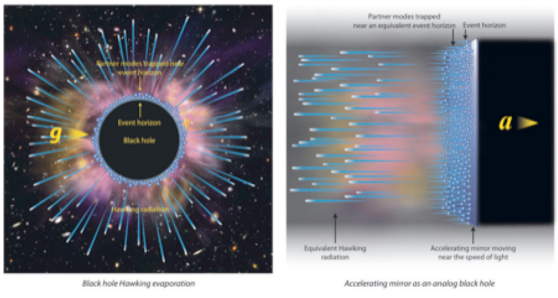

Figure 17. Accelerating mirror as an analog black hole. Left: Black hole Hawking evaporation and the trapping of the partner modes near the horizon. Right: An accelerating mirror also has a horizon and can also emit Hawking particles and trap their partner modes. The analogy between these two systems may be appreciated via Einstein's equivalence principle.

tions at their later stage and to reveal crucial details on how information may be preserved during black hole evaporation.

According to Einstein's equivalence principle, an accelerating mirror moving near the speed of light shares some common features with a true black hole (Einstein, 2002). In both cases, there exists an event horizon. Interacting with quantum fluctuations in vacuum near the horizon, both will emit Hawking particles and trap their partner modes (Fig. 17) until the black hole evaporates entirely or the accelerating mirror suddenly stops. By then the partner modes will be released. The purpose of this proposed experiment is to see whether and how the Hawking particles and their partners are entangled and therefore how the information would be preserved.

It is known that an intense laser traversing a plasma would push the intercepting plasma electrons to its back, the "plasma wakefields". Under extremely intense lasers, such density perturbations can be so concentrated that it can serve as a flying reflecting mirror. By properly tailoring the increase of the density of a thin-film target using nanofabrication technology, a relativistic plasma mirror accelerates as the driving laser continues to enter higher density regions. At the time when the laser leaves the thin-film target, the plasma mirror would abruptly stop its motion, which mimics the ending of the Hawking evaporation.

XII. TRANSMUTATION

Nuclear power wrestles with the problem of its spent fuel waste that still needs to be technically addressed (and a societal will needs to be forged). Among the three scenarios of nuclear waste disposal depicted in Fig. 18, i.e. (1) The no reprocessing approach (requiring 130,000 years for storage); (2) The spent fuel reprocessing (10,000 year storage requirement); and (3) The transmutation (which shortens the need for storage to 300 years and reduces the volume requirement by 100 times), one can find a laser-assisted path that allows for approach (3), which may be the most environmentally forward-looking.

The vision and its technology based on the combination of a CPA high power laser amplified within an OPCPA configuration by a pump created from efficient, high fluence fibre laser technology permits a new high repetition rate laser-driven neutron source for transmutation shown in Fig. 19. The OPCPA laser irradiates a nanometric foil ejecting deuterons onto a thin target to generate energy efficient neutrons by the fusion of D-T. The nascent investigation of laser ion acceleration through the physics of the Coherent Acceleration of Ions by Laser (CAIL) method (Tajima et al., 2009; Steinke et al., 2010) opens an efficient, compact, and economic path to the required neutron generation. Here CAIL introduces direct

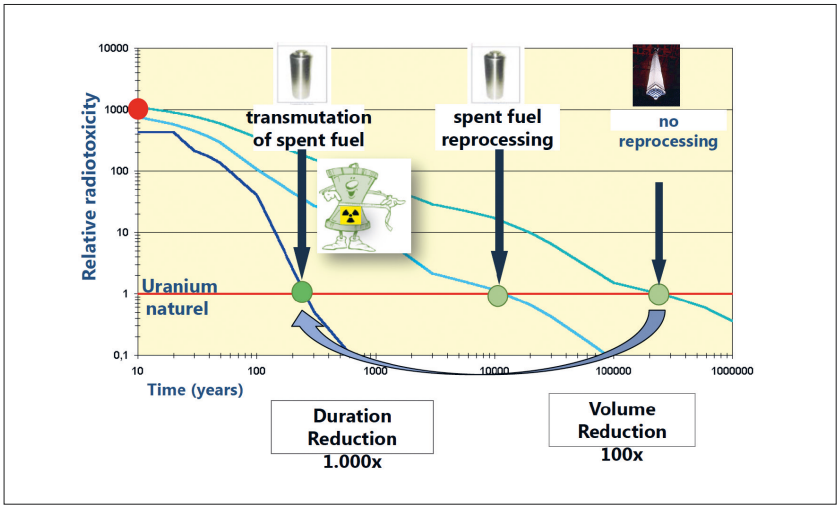

Figure 18. The radiotoxicity of spent nuclear fuel may be reduced from the level of no reprocessed case by about 1000 times if we transmute the spent fuel. This is why a substantial benefit may be gained by the transmutation. (Gales, 2018; Nifenecker et al., 2003).

ponderomotive acceleration of a thin sheet of electrons by the short-pulse laser, which in turn directly pulls ions behind the electrons. The condition of the resonant thinness of the target (and its limited mass) with the matched laser pulse intensity is the distinguishing feature of CAIL from the convention approach of Target Normal Sheath Acceleration, TNSA, (Snavely et al., 2000) in which electrons are heated by the laser absorption and no specific target mass relation exists to the laser intensity.

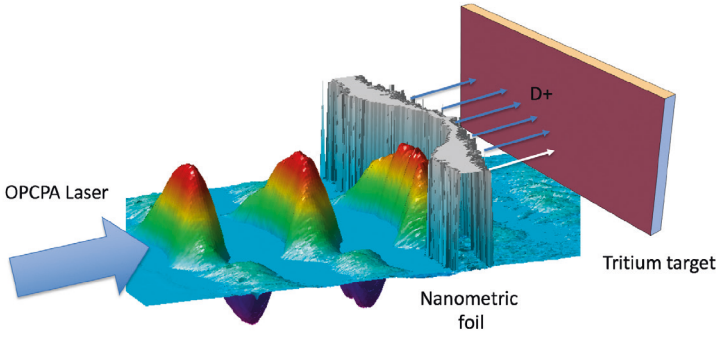

Figure 19. Neutrons are generated by an OPCPA laser irradiation of a nanometric deuteron foil, deuteron acceleration and interaction with tritiated solid target (Yan *et al.*, 2009).

The simulation of the CAIL process has been performed with the EPOCH PIC code (Brady et al., 2011). A linearly polarised laser of intensity 7.7×10^{17} W/cm^2 and wavelength 1 micron h been focused into a 3 micron beam footprint; this corresponds to $a_0 = 0.8$ where $a_0 = eE/(m_e c \omega_0) = 0.85\lambda_L(I/10^{18})^{1/2}$ where λ_L is the laser wavelength in μm and I is the laser intensity in W/cm^2. The foil is composed of deuterium with a target density of 1.0×10^{23} cm^{-3}. The efficiency of the energy conversion from the laser to ions of 20% has been shown numerically and it sensitively depends on the pulse length and target thickness. It has been shown previously (Steinke et al., 2010) that $a_0 = \sigma$ results in the highest efficiency where $\sigma = n_e/n_{cr} \cdot d/\lambda_L$ where ne is the electron density, n_{cr} the critical density ($= m_e \omega_L^2/4\pi e^2 = 1.1 \times 10^{21}/\lambda^2$ μm where ω_L is the laser frequency and λ μm is the laser wavelength in μm), d is foil thickness and λ_L is laser wavelength. The theoretically maximum energy is given under the optimal condition of $\sigma = a_0$ as

$$\epsilon_{max} = (2\alpha + 1)Qmc^2(\sqrt{a_0^2 + 1} - 1) \qquad (12)$$

Such research opens the way to aspire for the future application of emerging laser technology toward the practical transmutation technology of nuclear waste.

XIII. FEMTOSECOND OPHTHALMOLOGY

CPA-based lasers have attracted significant interest as their potential for high-precision micromachining due to the low damage threshold and deterministic character of the interaction. Surgical applications, particularly in the transparent delicate cornea or lens in the case of a cataract, can take maximal advantage of these attributes. By improving existing procedures and enabling entirely new ones, femtosecond laser technology has the potential to become the preferred corneal laser scalpel in the 21st century.

Corneal laser surgery to correct myopia (short-sightedness), hyperopia (far-sightedness) and astigmatism is becoming the most commonly performed medical laser procedure. Most techniques rely on altering the curvature of the cornea by removing corneal tissue using direct photoablation with ultraviolet light from the excimer laser. Two techniques have demonstrated a high degree of clinical efficacy, photorefractive keratectomy (PRK) and laser-assisted in situ keratomileusis (LASIK).

LASIK has gained recent popularity due to its minimal effect on the corneal surface, which reduces pain and recovery time. However, LASIK

requires the use of a mechanical blade (microkeratome) to give the excimer laser access to deeper corneal layers. In contrast to photoablative lasers, photodisruptive lasers operate in the near-infrared spectrum and are not absorbed (at least to the first order) in ocular media. Near-IR pulses can pass through transparent and limited thickness translucent material, affecting tissue only at the focus of the laser beam. In photodisruption, tissue effects are initiated by laser-induced optical breakdown (LIOB), which requires a small focal spot size to achieve a threshold fluence (energy/area) for plasma formation. Generation of a microplasma allows the target to absorb additional laser energy.

A. Optical Breakdown Energy Thresholds

An approximately square root dependence of the fluence threshold on the pulse duration is observed for pulses longer than 10 ps, below this value the dependence weakens significantly. Recent measurements down to 20-fs pulse durations have again confirmed these observations in corneal tissue (Loesel et al., 1999). These results suggest an optimal pulse duration for a corneal photo-disruptive laser in the few hundred femtosecond pulse duration range, where energy deposited in the tissue is significantly reduced. See Fig. 20. Further reduction of the laser pulse duration to a sub 100-fs level adds significant technical complexity and does not produce any further significant decrease of the threshold.

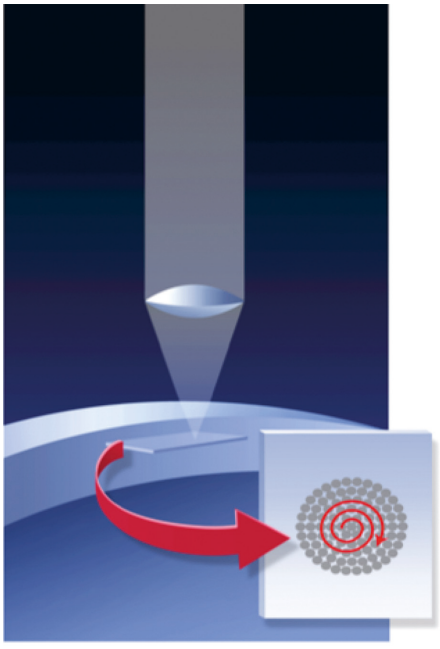

Figure 20. Intrastomal cut showing the importance of the pulse shortness: (a) 50 ps, (b) 100 fs. The picosecond laser cut is of poorer quality, manual dissection required to produce corneal cuts. The femtosecond laser produces a contiguous cut with surface quality similar to mechanical blades.

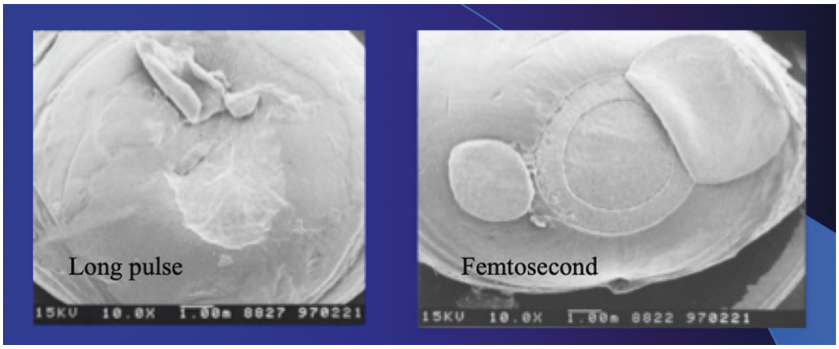

Figure 21. Femtosecond intrastromal scalpel.

B. Corneal Flap Cutting Procedure

(Squier et al., 1995; Ratkay-Traub et al., 2001)
Conventionally, a corneal flap is created with a mechanical microkeratome, a small motorised knife, to give the excimer laser access to deeper layers of the stroma during LASIK. For femtosecond laser-flap cutting (Fig. 21), the laser focus first is scanned along a spiral pattern inside the corneal stroma at a predetermined depth. The intrastromal cut is followed by several semi-circular shaped cuts at decreasing depth in the cornea to connect this intrastromal cut to the corneal surface, with a hinge present to maintain connection to the cornea. The depth is changed by movement of the focusing objective mediated by a computer-controlled galvo with accuracy of a few micrometers and speed that can accommodate a 10-kHz repetition rate. After the completion of the laser procedure, the contact glass is removed and the flap lifted, similar to what is done in the mechanical procedure. The technique offers some important advantage.

1. A decrease in LASIK flap complications.
2. Higher precision thickness of flap and residual tissue bed safe thin flaps.
3. Flexible hinge and bed parameters.
4. Planar flap, wavefront indicates less flap induced aberrations.

Immediate completion of interrupted procedures.

C. Extension of Corneal Flap Cutting to Corneal Transplants

The technique of flap cutting can readily be extended to corneal transplants procedures affecting 45,000 patients in the US. As shown in the Fig. 22, below, it can advantageously replace the trephines. It is not limited to full thickness transplants and can make easily partial thickness ones, 24a. Moreover, it can also create complex shapes, 24b, permitting self-locking that requires extensive suturing with a reduced healing time.

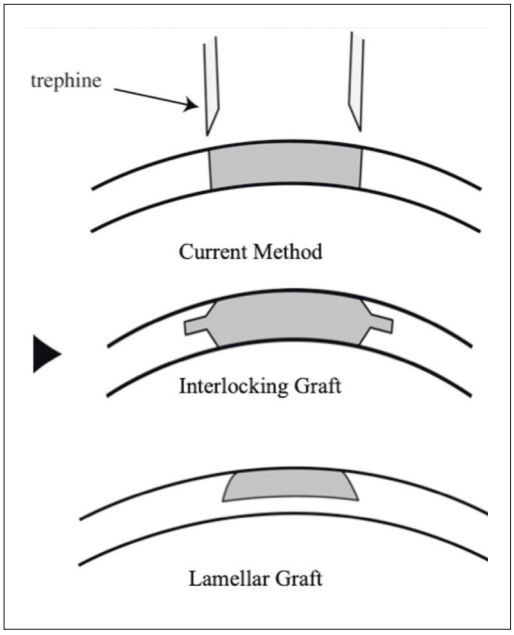

Figure 22. Today corneal transplant with trephine can only do a full thickness transplant. However, a femtosecond scalpel makes possible an interlocking graft. It shows also that a femtosecond laser can make a lamellar slice possible.

XIV. CONCLUSION

CPA has revolutionised the field of optics by providing the largest fields, the largest pressures, the largest temperatures and accelerations. The range of its applications has been considerable starting from the eV, the visible photon energy, and extending to the GeV, possibly the TeV. It is enlarging the field of optics from atomic to subatomic physics to include nuclear physics, high energy particle physics, astrophysics and cosmology. The applications are remarkably ubiquitous, going from the simple micromachining and eye surgery to the fundamental with TeV energy, like astrophysics, cosmology, gravitation or nonlinear QED. At intensities slightly above the solid or tissue damage threshold, it can be the perfect scalpel, cutting without any collateral damage. Through its interaction with gas, plasma, and solids, CPA can become a universal source of high energy radiations and particles. High harmonic generation in gases can yield attosecond X-UV pulses. The strength of its wake field in plasmas is such that it can accelerate particle with formidable gradients of GeV /cm, thousand times larger than conventional accelerating technique. The large energy acceleration provided by the laser through the Einstein equivalence principle, can be used to simulate a black hole and study, for instance, the loss of information paradox in a black hole. In addition, the electron being accelerated by a CPA laser in a gas can become by its lateral motion a powerful betatron source that emits radiation in the keV to

100 keV regime. Interacting with a solid target, high energy protons can be also efficiently produced. At very high intensity, the protons can become relativistic at an energy of 1 GeV. The protons in turn can produce neutrons. The latter can find a number of applications in the medical field like proton therapy or the production of nuclides for nuclear pharmacology. High energy protons can also be utilised for transmuting radiotoxic elements such as minor actinides which compose 60,000 metric tons of nuclear waste worldwide.

The CPA System provides ultra-high peak power in the PW level. However due to its low repetition rate in the Hz regime, its average power is in the 10–100 W range; which is far from enough for the applications such as particle collider or nuclear waste treatment. In addition, it is still plagued by a major flaw i.e, a very poor wall-plug efficiency of <1%. In this document we describe the project CAN which has the capability to provide both peak power, average power and efficiency.

Going to the Schwinger limit and beyond finally, current technology seems to limit the focused peak intensity to 10^{25} W/cm^2. To go higher, a novel compression technique is needed and presented. The intensity is obtained not by an augmentation of the energy but by the reduction of the laser pulse duration to the single cycle. By using relativistic mirrors, a gigantic ponderomotive force in the X-ray regime can be created with pulses as short as a zepto–attosecond. Once tightly focused it could easily produce intensity at or above the Schwinger limit. The ultra-high intensity could engender in a solid density a wake field with an acceleration gradient of TeV/cm, opening a fundamentally new vista beyond the Schwinger regime.

REFERENCES

1. Akhmanov, S. A., V. A. Vysloukh, and A. S. Chirkin, 1992, *Optics of Femtosecond Laser Pulses* (American Institute of Physics).
2. Albertazzi, B. et al., *Science* **346**, 325 (2014)
3. Arnould, M. et al., *Phys. Rept*. **450**, 97 (2007)
4. Aoyama, A., J. Ma, Y. Akahane, N. Inoue, H. Ueda, H. Kiriyama, K. Yamakawa, 2002, in *Technical Digest of Conference on Lasers and Electro-Optics* (CLEO) 2002 "Optical Society of America", p. 109.
5. Backus, S., C. Durfee, G. Mourou, H. C. Kapteyn, and M. M. Murnane, 1997, *Opt. Lett*. **22**, 1256.
6. Badziak, J., E. Woryna, P. Parys, K. Y. Platanov, S. Jablonski, L. Ryc, A. B. Vankov, and J. Wolowski, 2001, *Phys. Rev. Lett.* **87**, 215001.
7. Baetsle, L. H. et al., "Partitioning and transmutation in a strategic perspective," *Euradwaste*, **99**, 138 (2000).
8. Baltuška, A., T. Udem, M. Uiberacker, M. Hentschel et al., *Nature* **421**, 611 (2003).

9. Barty, C. P. J., C. L. Gordon III, and B. E. Lemoff, 1994, *Opt. Lett*. **19**, 1442.
10. Beaud, P., M. Richardson, E. Miesak, and B. T. Chai, 1993, *Opt. Lett.* **18**, 1550.
11. Bespalov, V. I., and V. I. Talanov, 1966, *JETP Lett.* **3**, 307.
12. Brabec, T., and F. Krausz, 2000, *Rev. Mod. Phys*. **72**, 545.
13. Brady, C. S. and T. D. Arber, "An ion acceleration mechanism in laser illuminated targets with internal electron density structure," *Plasma Phys. Control. Fusion*, 53, 074004 (2011).
14. Bula, C., K. T. McDonald, E. I. Prebys, et al., 1996, *Phys. Rev.Lett.* **76**, 3116.
15. Bulanov, S. V., and V. S. Khoroshkov, 2002, *Plasma Phys. Rep.* **28**, 453.
16. Bunkenburg, J., et al., 1985, *IEEE J. Quantum Electron*. QE-17, 1620.
17. Calegari, F., D. Ayuso, A. Trabattoni, L. Belshaw et al., *Science* 346, 336–339 (2014).
18. Calegari, F., G. Sansone, S. Stagira, C. Vozzi, M. Nisoli, J. Phys. B **49**, 062001 (2016).
19. Carman, R. L., R. F. Benjamin, and C. K. Rhodes, 1981, *Phys. Rev.* A **24**, 2649.
20. Cavalieri, A.L., N. Müller, Th. Uphues, V. S. Yakovlev et al., *Nature* **449**, 1029 (2007).
21. Cederbaum, L. S., J. Zobeley, Chem. *Phys. Lett.* **307**, 205 (1999).
22. Chen, P. and G. Mourou, 2017, "Accelerating Plasma Mirrors to Investigate the Black Hole Information Loss Paradox," *Phys. Rev. Lett.* **118**, 045001
23. Chen, S.N. et al., *Phys. Rev. Lett*. **108**, 055001 (2012)
24. Chen, S.N. et al., submitted to *Matter and Radiation at Extremes* (2018).
25. Clayton et al *Phys. Plasmas.* **1**, p1753 (1994).
26. Collier, J., C. Hernandez-Gomez, I. N. Ross, P. Matousek, C. N. Danson, and J. Walczak, 1999, *Appl. Opt.* **38**, 7486.
27. Collier, J. L., et al., 2004, unpublished.
28. Corkum, P.B., *Phys. Rev. Lett.* **71**, 1994 (1993).
29. Cousens, S., B. Reville, B. Dromey, and M. Zepf, "Temporal Structure of Attosecond Pulses from Laser-Driven Coherent Synchrotron Emission," *Phys. Rev. Lett.* **116**, 1–5 (2016).
30. Couture, A. and R. Reifarth, At. *Data Nucl. Data Tables* **93**, 807 (2007)
31. Cowan, J. J., et al. *Astrophys. J.* **294**, 656 (1985)
32. Ditmire, T., and M. D. Perry, 1993, *Opt. Lett.* **18**, 426.
33. Dubietis, A., G. Jonusauskas, and A. Piskarskas, 1992, *Opt. Commun.* **88**, 437.
34. Dudovich, N., O. Smirnova, J. Levesque, Y. Mairesse et al., *Nature Phys.* **2**, 781 (2006).
35. Duguay, M. A. and G. P. Rentzepis, *Appl. Phys. Lett.* 10, 350–352 (1967).
36. Einstein, A. and A. Engel. *The Collected Papers of Albert Einstein* Vol 7: The Berlin Years: Writings, 1918–1921. Princeton University Press, 2002.
37. Endoh, A., M. Watanabe, N. Sarukura, and S. Watanabe, 1989, *Opt. Lett*. **14**, 353.
38. Esarey, *IEEE Trans. Plasma Sci.* **24** p252 (1996).
39. Esirkepov, T., M. Borghesi, S. V. Bulanov, G. Mourou, and T. Tajima, 2004, *Phys. Rev. Lett*. **92**, 175003.
40. Everett et al *Nature* **368** p527 (1994).
41. Faure et al, *Nature* **431** p541 (2004).
42. Fourkal, E., B. Shahine, M. Ding, J. S. Li, T. Tajima, and C.-M. Ma, 2002, *Med. Phys*. **29**, 2788.
43. Fuchs, J. et al., *Nature Phys.* **2**, 48 (2006).
44. Gales, S., "Nuclear Energy and Waste Transmutation with High Power Accelerator and Laser Systems." [Online]. Available: https://indico.cern.ch/

event/617648/contributions/2517094/attachments/1442136/2220662/18_GALES_IZEST-Talk-Nuclear-Transmutation-040417.pdf. [Accessed: 22-Apr-2018].
45. Gauthier, J. et al, *Eur. Phys. Jour. D*, **48**, 3, 459-463 (2008).
46. Gauthier, D. et al, *Nature Communication*, **7**, 13688 (2016).
47. Geddes et al, *Nature* **431** p538 (2004).
48. Godet, J.P. et al, *Opt. Lett.*, **34, 16**, 2438-2440, 2009.
49. Gregori, G. et al., *Nature* **481**, 480–483 (2012).
50. Grischkowsky, D., A, C. Ballant, 1982, "Optical pulse compression based on enhanced frequency chirping," *Applied Physics Letters*, **41**.
51. Gumbrell, E. T. et al, New. *J. Phys*. **10**, 123011 (2008).
52. Hamm, R. (2010). Paper AP/IA-12, IAEA Proceedings Series, STI/PUB/1433, ISBN 978-92-0-150410-4.
53. Hentschel, M., R. Kienberger, Ch. Spielmann, G.A. Reider et al., *Nature* **414**, 509 (2001).
54. INTERNATIONAL ATOMIC ENERGY AGENCY, *Implications of Partitioning and Transmutation in Radioactive Waste Management*, no. 435. Vienna: INTERNATIONAL ATOMIC ENERGY AGENCY, 2004.
55. Jones, D.J., S.A. Diddams, J.K. Ranka, A. Stentz et al., *Science* **288**, 635 (2000).
56. Klünder, K., J. M. Dahlström, M. Gisselbrecht, T. Fordell et al., *Phys. Rev. Lett.* **106**, 143002 (2011).
57. Kmetec, J. D., J. J. Macklin, and J. F. Young, 1991, *Opt. Lett.* 16, 1001.
58. Kraus, P. M., B. Mignolet, D. Baykusheva, A. Rupenyan et al., *Science* **350**, 790 (2015).
59. Larsson, J., P. A. Heimann, A. M. Lindenberg, P. J. Schuk, P. H. Bucksbaum, R. W. Lee, H. A. Padmore, J. S. Wark, and R. W. Falcone, 1998, *Appl. Phys. A: Mater. Sci. Process.* **66**, 587.
60. Loesel, F.H., Tien, A.-C., Backus, S., et al., 1999, *Proc. SPIE*, 3565.
61. Lucchini, M., S. A. Sato, A. Ludwig, J. Herrmann et al., *Science* **353**, 916 (2016).
62. Luk, T. S., A. McPherson, G. Gibson, K. Boyer, and C. Rhodes, 1989, *Opt. Lett.* **14**, 1113.
63. Macchi, A., M. Borghesi, and M. Passoni, "Ion acceleration by superintense laser-plasma interaction," Rev. *Mod. Phys*. **85**, 751–793 (2013).
64. Maine, P., and G. Mourou, 1988, *Opt. Lett.* **13**, 467.
65. Maine, P., D. Strickland, P. Bado, M. Pessot, and G. Mourou, 1987, *Rev. Phys. Appl.* 22, 1657.
66. Maine, P., D. Strickland, P. Bado, M. Pessot, and G. Mourou, 1988, IEEE J. *Quantum Electron.* **24**, 398.
67. Mangles et al, *Nature* **431** p535 (2004).
68. Martinez, O. E., 1987, *IEEE J. Quantum Electron.* 23, 1385.
69. Migus, A., C. V. Shank, E. P. Ippen, and R. L. Fork, 1982, *IEEE J. Quantum Electron.* QE-18, 101.
70. Mourou, G., T. Tajima, and S. Bulanov, 2006, "Optics in the relativistic regime," *Rev. Mod. Phys*., **78**, 2, p 309.
71. Mourou, G., B. Brocklesby, T. Tajima, and J. Limpert, 2013, "The future is fibre accelerators," *Nature Photonics* **7**, p 258.
72. Mourou, G., S. Mironov, E. Khazanov, and A. Sergeev, 2014, "Single cycle thin film compressor opening the door to Zeptosecond-Exawatt physics," *Eur. Phys. J. Spec. Top.*, **223**, 6, p1181.
73. Mumpower, M.R. et al., *Progr. in Part. And Nucl. Phys.* **86**, 86 (2016).
74. Nakatsutsumi, M. et al., *Optics Lett*. **35**, 2314–2316 (2010).

75. Nakatsutsumi, M. et al., *Nat. Comm.* **9**, 280 (2018).
76. Naumova, N. M., J. A. Nees, I. V. Sokolov, B. Hou, and G. A. Mourou, 2004, "Relativistic generation of isolated attosecond pulses in a lambda-cubed focal volume," *Phys. Rev. Lett*. **92**, 063902.
77. Naumova, N., I. Sokolov, J. Nees, A. Maksimchuk, V. Yanovsky, and G. Mourou, 2004, *Phys. Rev. Lett.* **93**, 195003.
78. Naumova, N. M., J. A. Nees, B. Hou, G. A. Mourou, and I. V. Sokolov, 2004, "Isolated attosecond pulses generated by relativistic effects in a wavelength-cubed focal volume," *Opt. Lett.* **29**, 778.
79. Nees, J., S. Biswal, F. Druon, J. Faure, M. Nantel, and G. Mourou, 1998, *IEEE J. Sel. Top. Quantum Electron*. **4**, 376.
80. Nifenecker, H., O. Meplan, and S. David, *Accelerator driven subcritical reactors*. CRC Press, 2003.
81. Nisoli, M., S. De Silvestri, O. Svelto, *Appl. Phys. Lett.* **68**, 2793 (1996).
82. Nisoli, M., De Silvestri, S., Svelto, O., Szipöcs, R., Ferencz, K., Spielmann, Ch., Sartania, S. & Krausz, F., 1997, "Compression of High-Energy Laser Pulses below 5fs," *Opt. Letters* **22**, 522.
83. Oliva, E. et al *Nature Photonics* **6**, 764–767 (2012).
84. Ossiander, M., F. Siegrist, V. Shirvanyan, R. Pazourek et al., *Nature Phys*. **13**, 280 (2017).
85. Panov, I.V., *Phys. of Atomic Nuclei* **79**, 159–198 (2016).
86. Paul, P.M., E.S. Toma, P. Breger, G. Mullot et al., *Science* **292**, 1689 (2001).
87. Perry, M., P. Pennington, B. C. Sutuart, et al., 1999, *Opt. Lett*. **24**, 160.
88. Pessot, M., J. Squier, and G. Mourou, 1989, *Opt. Lett.* **14**, 797.
89. Pessot, M., et al., 1987, *Opt. Commun*. **62**, 419.
90. Potemkin, A. K., M. A. Martyanov, M. S. Kochetkova, and E. A. Khazanov, 2009, "Compact 300 J/ 300 GW frequency doubled neodimium glass laser. Part I: Limiting power by self-focusing," *IEEE Journal of Quantum Electronics* **45**, 336.
91. Pretzler, G. et al., *Phys. Rev*. E **58**, 1165 (1998).
92. Ratkay-Traub I1, Juhasz T, Horvath C, Suarez C, Kiss K, Ferincz I, Kurtz R., Ultra-short pulse (femtosecond) laser surgery: initial use in LASIK flap creation. Ophthalmol Clin North Am. 2001 Jun;14 (2):347–55, viii–ix.
93. Reifarth, R. et al., *J. Phys. G: Nucl. Part. Phys*. **41**, 053101 (2014).
94. Remacle, F., R. D. Levine, *Proc. Natl. Acad. Sci. U.S.A*. **103**, 6793 (2006).
95. Remington, B. A., et al. *Science* **284**, 1488 (1999)
96. Ross, I. N., J. L. Collier, P. Matousek, et al., 2000, *Appl. Opt*. **39**, 2422.
97. Ross, I. N., et al., 1997, *Opt. Commun*. **144**, 125.
98. Roth, M., et al., 2001, *Phys. Rev. Lett.* **86**, 436.
99. Rouyer, C., et al., 1993, *Opt. Lett.* **18**, 214.
100. Rynes, J. et al., *Nucl. Instrum. Meth*. A **422**, 895 (1999).
101. Sansone, G., L. Poletto, M. Nisoli, *Nature Photon.* **5**, 655 (2010).
102. Sansone G., F. Kelkensberg, J. F. Pérez-Torres, F. Morales et al., *Nature* **465**, 763-766 (2010).
103. Schafer, K.J., B. Yang, L.F. DiMauro, K.C. Kulander, *Phys. Rev. Lett.* **70**, 1599 (1993).
104. Schiffrin, A., T. Paasch-Colberg, N. Karpowicz, V. Apalkov et al., *Nature* **493**, 70 (2013).
105. Schlaepfer, F., M. Lucchini, S. A. Sato, M. Volkov et al., *Nature Phys.* **14**, 560 (2018).

106. Schoenlein, R. W., S. Chattopadhyay, H. H. W. Chong, et al., 2000, *Science* **287**, 2237.
107. Schultze, M., M. Fieß, N. Karpowicz, J. Gagnon et al., *Science* **328**, 1658 (2010).
108. Schultze, M., E.M. Bothschafter, A. Sommer, S. Holzner et al., *Nature* **493**, 75 (2013).
109. Schultze, M., K. Ramasesha, C.D. Pemmaraju, S.A. Sato et al., *Science* **346**, 1348 (2014).
110. Siegman, A. E., 1986, *Lasers* University Science Books, Mill Valley, CA", p. 362.
111. Snavely, R. et al., "Intense high energy proton beams from petawatt-laser irradiation of lasers", *Phys. Rev. Lett*. 85, 2945 (2000).
112. Squier, J., F. Salin, G. Mourou, and D. Harter, 1991, *Opt. Lett*. 16, 324.
113. Squier, Du, J., Kurtz, R.M., Elner, V., et al., 1995, in *Ultrafast Phenomena IX*, Barbara, P.F. et al., Ed. (New York: Springer), 254.
114. Steinke, S. et al., "Efficient ion acceleration by collective laser-driven electron dynamics with ultra-thin foil targets," *Laser Part. Beams*, **28**, 215 (2010).
115. Strickland, A. D., and G. Mourou, 1985, *Opt. Commun*. **56**, 212.
116. Sullivan, A., et al., 1991, *Opt. Lett*. **16**, 1406.
117. Tajima T and Dawson J. M., *Phys. Rev. Lett*. **43**, 267 (1979)
118. Tajima, T., D. Habs, and X. Yan, "Laser Acceleration of Ions for Radiation Therapy," *Rev. Accel. Sci. Technol.*, **2**, 201 (2009).
119. Telnov, V. I., 1990, *Nucl. Instrum. Methods Phys. Res.* A **294**, 72.
120. Telnov, V. I., 2000, *Int. J. Mod. Phys.* A **15**, 2577.
121. Telnov, V. I., 2001, *Nucl. Instrum. Methods Phys. Res.* A **472**, 43.
122. Teubner, U. and P. Gibbon, *Reviews of Modern Physics* (2008).
123. Thielemann, F.-K. et al., Progr. in *Part. And Nucl. Phys.* **66**, 346–353 (2011)
124. Treacy, E. B., 1969, *IEEE J. Quantum Electron*. **5**, 454.
125. Tsakiris, G. D. et al, *New Journal of Physics,* **8**, 19 (2006).
126. Uiberacker, M., Th. Uphues, M. Schultze, A.J. Verhoef et al., *Nature* **446**, 627 (2007).
127. Vaillancourt, T. G., B. Norris, J. S. Coe, and G. A. Mourou, 1990, *Opt. Lett*. **15**, 317.
128. Van der Meer, K., et al., *Nucl. Instrum. Methods Phys. Res. Sect.* B **217** 202–220 (2004).
129. Vodungbo, B. et al, *Optics Express,* **19**, 5, 4346 (2011).
130. Wang, Y. et al, *Nature Photonics,* **8**, 381 (2014).
131. Wulff, M., D. Bourgeois, T. Ursby, L. Goir, and G. Mourou, 1997, in *Time Resolved Diffraction*, edited by J. R. Helliwell and P. M. Rentzepis (Clarendon Press, Oxford), pp. 195–228.
132. Yamakawa, K., H. Shiraga, Y. Kato, and C. P. J. Barty, 1991, "Prepulse-free 30-TW, 1-ps Nd:glass laser," *Optics Letters* **16**, 1593.
133. Yan, X. Q., T. Tajima, M. Hegelich, L. Yin, and D. Habs, "Theory of laser ion acceleration from a foil target of nanometer thickness," *Appl. Phys. B Lasers Opt.* **98**, 711–721 (2010).
134. Yokoya, K., 2000, *Nucl. Instrum. Methods Phys. Res*. A **455**, 25.
135. Zeitoun, P. et al, *Nature*, **431**, 426 (2004).
136. Zhou, M. L., X. Q. Yan, G. Mourou, J. A. Wheeler, J. H. Bin, J. Schreiber, and T. Tajima, "Proton acceleration by single-cycle laser pulses offers a novel monoenergetic and stable operating regime," *Phys. Plasmas* **23**, 43112 (2016).